Research Square

Preprints are preliminary reports that have not undergone peer review.
They should not be considered conclusive, used to inform clinical practice,
or referenced by the media as validated information.

Hydrothermal Functionalization and Characterization of Bambusa vulgaris Biochar for High-Efficiency Electrostatic Adsorptive Removal of Reactive Black 5 Dye from Wastewater

Ehigbochie Joy Ofure
University of Science and Technology of China
Guijian Liu
nrj661@mail.ustc.edu.cn

University of Science and Technology of China
Ruijia Liu
University of Science and Technology of China
Yuan Liu
University of Science and Technology of China
Balal Yousaf
Silesian University of Technology

Research Article

Keywords: Bamboo biochar, Ammonia functionalization, Reactive Black 5, Adsorption, Wastewater treatment, Dye pollution

Posted Date: April 17th, 2026

DOI: https://doi.org/10.21203/rs.3.rs-8302820/v1

License: This work is licensed under a Creative Commons Attribution 4.0 International License.
Read Full License

Additional Declarations: No competing interests reported.

Version of Record: A version of this preprint was published at Water, Air, & Soil Pollution on July 8th, 2026. See the published version at https://doi.org/10.1007/s11270-026-09697-6.

Hydrothermal Functionalization and Characterization of *Bambusa vulgaris* Biochar for High-Efficiency Electrostatic Adsorptive Removal of Reactive Black 5 Dye from Wastewater

Ehigbochie Joy Ofure[a], Guijian Liu[a]*, Ruijia Liu[a] , Yuan Liu[a], Balal Yousaf[b]

[a]*CAS-Key Laboratory of Crust-Mantle Materials and the Environment, School of Earth and Space Sciences, University of Science and Technology of China, Hefei 230026, PR China.*

[b]*Department of Technologies and Installations for Waste Management, Faculty of Energy and Environmental Engineering, Silesian University of Technology,44-100, Gliwice, Poland.*

* Corresponding author. Tel: +86-551-63603714; Fax: +86-551-63621485.

Email address: nrj661@mail.ustc.edu.cn (Guijian Liu)

Abstract

Water pollution by synthetic dyes has become a serious environmental concern due to their toxicity, persistence, and widespread discharge from textile and related industries. Among these dyes, reactive black 5 (RB5) is commonly detected in industrial effluents and poses significant risks to aquatic ecosystems and human health. In this study, we investigated the adsorptive removal of RB5 from aqueous solutions using *Bambusa vulgaris* biochar modified with varying concentrations of ammonia. Bamboo biochar (BB) was prepared via pyrolysis and further functionalized using 20- and 30-mL ammonia treatments to produce B20 and B30, respectively. All prepared adsorbents were comprehensively characterized using SEM, BET, FTIR, TGA, CHN, XRD, and XPS to better understand their physicochemical properties. Adsorption studies systematically examined the effect of contact time, solution pH, adsorbent dose, and initial dye concentration. B20 and B30 exhibited consistently greater initial RB5 dye removal efficiencies (B20: 92.5%; B30: 89.8%) and rates compared to BB (75.2%), with optimum performance at acidic pH. Kinetics were best fitted to the Pseudo-First-Order model, but equilibrium data were best represented by the Langmuir isotherm model, confirming monolayer sorption. The recyclability of BB, B20, and B30 was tested for 8 successive adsorption-desorption cycle. The biochar modified by ammonia presented considerably enhanced recyclability and stability. B20 and B30 retained 67.8% and 66.2% of their initial efficiency, respectively, compared to BB's 48.5%. After-adsorption characterization was done using elemental analysis, FTIR, XRD, SEM, XPS, BET which confirmed RB5 adsorption. This study reveals the immense potential of ammonia-functionalized *Bambusa vulgaris* biochar, particularly B20, as a highly effective, reusable, and environmentally friendly adsorbent for the successful treatment of anionic dye-polluted textile wastewater.

Keywords: Bamboo biochar, Ammonia functionalization, Reactive Black 5, Adsorption, Wastewater treatment, Dye pollution

1.0 Introduction

According to global data, about 359.4×10^9 m^3 of wastewater are produced annually, of which 63% (225.6×10^9 m^3) are collected and 52% (188.1×10^9 m^3) are treated. This suggests that approximately 48% of wastewater production globally is released into the environment unprocessed, which is a significant decrease from earlier predictions of almost 80%-(Jones et al., 2021). Among the many causes, dye discharge contributes significantly to water contamination. Due to their durability and affordability, over 9000 synthetic dyes are widely utilized in a variety of industries, including textiles, cosmetics, leather, paper, medicines, and food. Major dye pollutants include rhodamine B (RB), methylene blue (MB), malachite green, methyl orange (MO), rhodamine 6G, fuchsin basic, methyl violet, and eosin Y (Saad et al., 2023). When these dyes come into direct contact with the eyes, they can cause respiratory problems, skin irritation, and possibly irreversible damage. They can also be genotoxic and carcinogenic. Environmental dyes cause aquatic pollution, which impacts photosynthesis, oxygen levels, plant growth, and food chains (Mehra et al., 2021).

Among the different dye classes, RB5, an azo dye is notably problematic because of its high solubility, complicated aromatic structure, and resistance to traditional wastewater treatment technologies (Zheng et al., 2016). RB5 is a vinyl sulphone reactive dye that contains azo chromophores (figure 1). RB5 is also known as Remazol black B in the industry. Its significant popularity is owing to its relatively inexpensive cost, low energy consumption, bright color, and good stability (Karadag et al., 2007). Reactive dyes are often more stable than other types of dyes because they connect to target materials via covalent bonds, which significantly boosts colorization efficiency (Nematollahzadeh et al., 2015). RB5 can have a negative impact not just on the ecosystem, but also on human and animal health. Previous research suggested that continuous and prolonged exposure to RB5 could result in skin rashes, bladder cancer, chromosomal abnormalities, respiratory and kidney failure, blindness, shock, cardiovascular collapse, and asthma. In this perspective, the elimination of RB5 is quite important (Chang & Shih, 2018) (Shokohi et al., 2011).

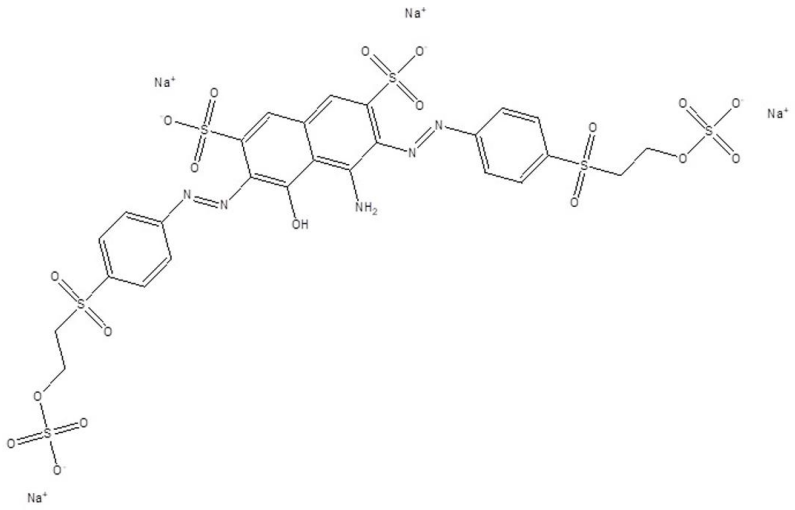


Figure 1: Chemical Structure of RB5 Dye (JALALI & Doroudi, 2020).

A broad variety of physical, chemical, and biological techniques, such as coagulation and flocculation (Verma et al., 2012), membrane separation (Moradihamedani, 2022), photocatalytic degradation (Kumari et al., 2023), biodegradation (Gao et al., 2018), and advanced oxidation processes (AOPs) have been explored for dye removal from wastewater (Ledakowicz & Paździor, 2021). However, these techniques frequently confront restrictions, including significant operational costs, secondary pollution, complex maintenance requirements, and inconsistent efficacy across various dye types and concentrations. Adsorption has emerged as the preferred technique for dye removal due to its simplicity, high efficiency, cost-effectiveness, and ability to remove a wide spectrum of contaminants without forming toxic by-products (Rashid et al., 2021). The adsorption process is a surface phenomenon in which adsorbates transfer to adsorbents. Adsorption technology has been widely used in water and wastewater treatment for decades due to its low cost, efficiency, simplicity, and environmental friendliness (Wang & Guo, 2020; Wekoye et al., 2020). Adsorption can achieve removal efficiencies of up to 99.9% (Anil et al., 2020; Wong et al., 2020).

Biochar, a carbon-rich material generated from the pyrolysis of biomass under oxygen-limited conditions, has received substantial interest for its potential as a sustainable adsorbent (Yuan et al., 2023). Its adsorption capability is mostly determined by its porosity nature and various functional groups like hydroxyl, carbonyl, and carboxyl (Niazi et al., 2016). Biochar is derived from plant biomass consists of hemicellulose, cellulose, and lignin, and its features are shaped by the varied pyrolysis rates, processes, and pathways of these components, resulting to diverse porosity structures and functional group forms (Z. Zhang et al., 2022). In recent years, agricultural wastes, such as wheat straw, cabbage and coconut waste,

peanut husk, pumpkin seed hulls, mango seed husks, cashew nutshell, bamboo, spent tea leaves, walnut shells, and orange peel, have been utilized to make carbon compounds that can absorb dye from wastewater (Amin et al., 2019) (Enaime et al., 2023). Bamboo, specifically *Bambusa vulgaris*, stands out as a promising biomass resource due to its rapid growth rate, high lignocellulosic content, and renewability (Aizuddin et al., 2023). The conversion of *Bambusa vulgaris* into biochar has a dual environmental benefit: decreasing waste biomass and producing low-cost adsorbents for wastewater cleanup (Alfei & Pandoli, 2024).

However, directly derived biochar from biomass pyrolysis has low surface area and pore volume, limited functional groups like carboxyl, carbonyl, and hydroxyl groups, and poor surface functionality (Zhou et al., 2018). These intrinsic drawbacks may lessen biochar's effectiveness as a useful substance. However, it is frequently possible to modify the pore volume and surface functionality of biochar, which enables the production of numerous functional materials (Singh et al., 2021). Alkaline amino groups on biochar's surface can greatly improve its efficacy in applications like organic pollutant adsorption. Amination modification of biochar can boost the adsorption performance and catalytic activity by introducing amino functional groups (Sajjadi et al., 2019);(Qin et al., 2019). It has been recognized that the hydrothermal process permits the production of even the toughest or most complicated material(s) with the appropriate physicochemical properties (Kambo & Dutta, 2015b). It has several advantages over other conventional processes, such as energy savings, simplicity, cost effectiveness, better nucleation control, pollution-free (because the reaction is carried out in a closed system), higher dispersion, higher rate of reaction, better shape control, and lower operating temperature in the presence of an appropriate solvent, etc (de Conti et al., 2023).

In a previous study, Kapoor et al. (2022) investigated the removal of RB5 dye from an aqueous solution via adsorption onto banana peel biochar. pH, exposure length, RB5 dye concentration, adsorbent dosage, particle size, and temperature were all studied. At pH 3 and 75 mg/L adsorbate concentration, banana peel biochar removed up to 97% of the RB5 dye. Characterization of the adsorbent material was carried out using Fourier transform infrared (FTIR) and scanning electron microscopy. The equilibrium data were evaluated using the Langmuir and Freundlich isotherm models. The Langmuir isotherm best represented the experimental results, with a maximum adsorption capacity of 7.58_mg/g. Kinetic parameters were investigated, and the pseudo-second order was found to be appropriate, indicating that the rate of adsorption was regulated by physisorption. In another study, Nguyen et al. (2021) used ultrasound technology to prepare biochar for RB5 removal. They modified the biochar in a short period of time using ultrasound cavitation, with no additional chemicals

required and no hazardous byproducts. As a result of this alteration, the surface area and pore volume tripled, as did the adsorption rate. Acidic pH favored RB5 removal because it increased the electrostatic interaction between the anionic dye and the positively charged charcoal. RB5 adsorption followed the Langmuir isotherm and was monolayer in nature, as evidenced by the high correlation coefficient of $R^2 = 0.999$. Chemisorption took place between RB5 and the adsorbent, following the pseudo-second-order kinetic model.

The aim of our study is to examine how well carbon-based adsorbents made from agricultural waste can adsorb and remove RB5 dye from aqueous solutions. Specifically, *Bambusa vulgaris* is selected as a sustainable and abundant feedstock for biochar production. The core objectives of this research involve a meticulous and comprehensive characterization of the *Bambusa vulgaris* biochar, its functionalization to enhance adsorption capabilities, and evaluating its efficacy in adsorbing RB5 dye within aqueous environments.

2.0 Materials and Methods

2.1 Chemicals and Materials

The *Bambusa vulgaris* biochar used in this study was obtained from China. Ammonia solution (NH_3, 25% w/v) used for hydrothermal functionalization of the biochar, was obtained from Alfa Aesar (China). Reactive Black 5 (RB5), an anionic azo dye commonly used in textile industries and selected as the target pollutant due to its high environmental persistence, was supplied by Alfa Aesar (China) and used as received. The molecular formula and molar mass of RB5 are $C_{26}H_{21}N_5Na_4O_{19}S_6$ and 991.82 $g \cdot mol^{-1}$, respectively. All glassware used in the experiments was soaked in 10% nitric acid (HNO_3), thoroughly rinsed with deionized water, and dried before use to eliminate any potential contamination. Weighing was conducted using an electronic analytical balance (±0.1 mg accuracy), and pH adjustments during batch adsorption experiments were done using 0.1 M NaOH and 0.1 M HCl solutions.

2.2 Preparation of Bambusa vulgaris Biochar

The *Bambusa vulgaris* biochar used in this study was produced via slow pyrolysis of dried bamboo culm at 500°C under oxygen-limited conditions and was stored in an airtight container prior to functionalization.

2.3 Hydrothermal Functionalization of Bambusa vulgaris Biochar

In this method, aqueous ammonia (NH_4OH) was used to introduce nitrogen-containing surface functionalities onto the bamboo biochar (denoted as BB). Specifically, 20 and 30 mL of ammonia solution were each diluted with 100 mL of distilled water in separate beakers. Each ammonia solution was thoroughly mixed with 50 g of pre-prepared bamboo biochar and stirred at room temperature at 25 °C for 30 minutes to establish homogeneity and sufficient surface contact. The suspensions were placed in Teflon-lined autoclave reactors, sealed, and hydrothermally treated in a muffle furnace at 180°C for 24 hours. Following the reaction, the autoclaves were left to cool naturally to ambient temperature. The treated biochar samples were then filtered and washed several times with distilled water until the filtrate achieved neutral pH. The biochars were oven-dried at 60°C overnight to eliminate moisture. This procedure was repeated for each ammonia concentration (20 and 30 mL), with the resulting samples labeled B20 and B30, respectively

2.4 Characterization of Functionalized Biochar

Various instrumental analyses were conducted in the central laboratory of the University of Science and Technology of China to investigate the properties of the functionalized biochar before and after adsorption. Elemental analysis was used to determine the carbon (C), hydrogen (H), and nitrogen (N) contents of *Bambusa vulgaris* biochar and functionalized composites. The CHN elemental analysis was performed using a Vario EL cube V2.0.3 instrument (manufactured by Elementar Analysen systeme GmbH). The morphologies and chemical compositions of the functionalized biochar were analyzed through Scanning Electron Microscopy (SEM). The pertinent SEM images were carefully selected to display the structural characteristics of the biochar. The Brunauer–Emmett–Teller (BET) method determined the specific surface areas, pore volumes, and pore sizes at relative pressures. The nitrogen adsorption-desorption measurements were conducted with Autosorb-6iSA and Quanta chrome Instruments (made in the US) to ascertain textural physiognomies such as pore sizes plus total pore volumes. The analyses of the surface functional groups before and after the adsorption of RB5 dye were carried out using Fourier-Transform Infrared Spectroscopy (FTIR) spectroscopy (Nicolet 6700 spectrometer), with wave numbers ranging between 4000 and 400 cm^{-1}. X-ray diffraction (XRD) was used to analyze the crystalline structure and phase composition of functionalized *Bambusa vulgaris* biochar samples using a X'Pert PRO diffractometer (Philips) equipped with a Cu Kα radiation source (λ = 1.5406 Å) with a scan range of 10◦ to 80◦(2θ). Thermal stability was measured using SDT Q600 (TA Instruments, USA), from 30 to 1000◦C in N2 at 10 ◦C/min. XPS analysis was used to explore the surface chemistry of *Bambusa vulgaris* biochar before and after functionalization using a Thermo Scientific K-Alpha XPS System. Microsoft Excel and Origin 2021 were utilized to create the graphs.

2.5 Batch Adsorption Experiments

Batch adsorption studies were carried out to determine the effect of various operational factors on the adsorption efficiency of RB5 onto produced *Bambusa vulgaris* biochar and functionalized composites. The studies were carried out in 50 mL conical flasks that were shaken on an orbital mechanical shaker at 153 rpm for 2 hours, unless otherwise noted. After adsorption, the solutions were filtered. The residual content of RB5 dye in the filtrates was evaluated using a UV-Visible spectrophotometer at a wavelength of maximum absorption (λmax) of 597 nm.

The adsorption capacity at equilibrium, qe (mg/g), was calculated using the following equation:

$$qe = \frac{(C_o - C_e)V}{m} \quad (1)$$

Where:

C_0 is the initial concentration of the dye solution (mg/L); Ce is the equilibrium concentration of the dye solution (mg/L); V is the volume of the dye solution (L) and m is the mass of the adsorbent (g).

2.5.1. Effect of Initial Dye Concentration

The influence of initial dye concentration on the adsorption process was examined by creating 20 mL of RB5 dye solutions with concentrations ranging from 3, 6, 9, 12, 15, 18, 21, 25, and 30 ppm. Each solution received 0.02 g of the produced adsorbent (pristine and functionalized biochar particles). The flasks were then shaken on an orbital mechanical shaker for two hours. After the adsorption period, the solutions were filtered, and the filtrates were examined using a UV-visible spectrophotometer at 597 nm to measure the equilibrium dye concentration.

2.5.2. Effect of pH

To identify the ideal pH for RB5 dye adsorption, studies were carried out by altering the dye solution's starting pH. In 50 mL conical flasks, 0.02 g of biochar was used as an adsorbent and 20 mL of RB5 dye solution was added. The dye solutions' pH was changed to 1, 3, 5, 7, and 9 with dilute NaOH or HCl solutions. The flasks were then placed on the orbital shaker for 2 hours at 153 rpm. Following agitation, the filtrates were examined using a UV-visible spectrophotometer at 597 nm.

2.5.3. Effect of Contact Time

The effect of exposure time on RB5 dye adsorption was investigated in order to estimate the equilibrium time for the adsorption process. A 30 mg/L RB5 dye solution was utilized. Adsorption studies were conducted at various time intervals, including 15, 25, 35, 45, 60, 75, 90, 105, and 120 minutes. In 50 mL conical flasks, a set amount of adsorbent (0.02 g, determined by early concentration experiments) was introduced and stirred with 20 mL of the 30 mg/L RB5 dye solution. The solutions were sampled at each required time interval, filtered, and examined using a UV-visible spectrophotometer at 597 nm.

2.5.4. Effect of Adsorbent Dosage

The optimum adsorbent dose for efficient RB5 dye removal was determined by changing the amount of adsorbent added to a fixed volume and concentration of dye solution. Various doses of biochar (0.04, 0.06, 0.08, 0.1, 0.2, 0.4, 0.6, 0.8, and 1 g) were exposed to 20 mL of RB5 dye solution (at an optimal beginning concentration, e.g., 30 mg/L, as determined by earlier research). The mixures were shaken on an orbital shaker for two hours (equilibrium time). Following filtration, the residual dye concentration was determined using a UV-Visible spectrophotometer at 597 nm.

2.6. Adsorption Kinetics and Isotherm

2.6.1. Adsorption Kinetics

Adsorption kinetics analysis reveals the rate at which a solute is taken up. It determines the amount of time the adsorbate remains at the solution's interface. This rate is critical for the design of the adsorption system and can be calculated using kinetic analysis. The study of adsorption kinetics is significant because it provides the equilibrium (Damahe et al., 2024). To determine how contact time impacts adsorption, the kinetics were modeled using pseudo-first-order (PFO), Elovich, and intraparticle diffusion models. The correlation coefficients (R^2) were calculated after the models had been fitted to the experimental data. Each kinetic adsorption experiment's data was confirmed three times for correctness. These models help to understand the rate-limiting phases and the overall speed of the adsorption process.

2.6.1.1. Pseudo-First-Order Model

Lagergren's first-order rate equation is known as a pseudo first-order model because it distinguishes between kinetic equations and solution concentration based on adsorption capacity (Y. S. Ho et al., 2000). It is given by equation (2) below:

$$q_t = ((1 - \exp(-k_1 t)) \quad (2)$$

Where k_1 is the rate constant, q_t = amount adsorbed at time t (mg/g) and t= time (min)

2.6.1.2 Elovich Model

The Elovich model is based on the kinetic principle, which states that adsorption sites expand exponentially with adsorption, resulting in multilayer adsorption. Zeldowitsch developed the Elovich model to describe the chemical nature of adsorption. This model can help forecast a system's mass and surface diffusion, as well as its activation and deactivation energy. The concept has been employed in gaseous systems, but its applicability in wastewater treatment approaches have received significant interest (Alshabanat et al., 2013).

The Elovich equation is given as:

$$q_t = \frac{1}{\beta} In(1 + \alpha\beta t) \quad (3)$$

Where α = initial adsorption rate (mg/g.min), β = desorption constant; q_t = amount adsorbed at time t (mg/g) and t= time (min)

2.6.1.3 Intraparticle Diffusion Model

The intraparticle diffusion model can be used to investigate the removal of pollutants by an absorbent during a diffusion process (Lv *et al.,* 2018). This model has been used many times to examine the rate limiting step during adsorption. The adsorption of solute in a solution involves mass transfer of adsorbate (film diffusion), surface diffusion, and pore diffusion. A functional relationship that is common to most adsorption processes is that the uptake proportionally varies with $t^{½}$, the Webber-Moris plot (qt against $t^{½}$) rather than with time, t (Kaur *et al.,* 2013). The model can be expressed as:

$$q_t = k_{id}.t^{0.5} + C \quad (4)$$

Where qt= amount adsorbed at time t (mg/g); t= time (min); k_{id} =intraparticle diffusion rate constant (mg/g·$min^{0.5}$) and C= intercept (mg/g)

2.6.2. Isotherm Study

The adsorption isotherm describes how the adsorbate (RB5 dye) interacts with the adsorbent (biochar), as well as the relationship between adsorption capacity and adsorbate concentration at equilibrium. We can use isotherms to model equilibrium adsorption data and explore adsorption information, such as adsorption mechanisms, maximum adsorption

capacity, and adsorbent properties (Damahe et al., 2024; Wang & Guo, 2020). The experimental adsorption equilibrium data in this study were analyzed using well-known adsorption isotherm models such as the Langmuir, Freundlich, and Flory-Huggins.

2.6.2.1 Langmuir Isotherm

The Langmuir (1918) adsorption isotherm has long been used to characterize gas-solid phase adsorption (Davis et al., 2003). The Langmuir model is commonly used for batch biosorption data, and in most circumstances, it successfully describes the equilibrium of dye biosorption (Yagub et al., 2014). The nonlinear and linear Langmuir models are presented as following:

$$q_e = \frac{q_{max} K_L C_e}{1+K_L C_e} \quad (5)$$

$$\frac{C_e}{q_e} = \frac{C_e}{q_m} + \frac{1}{K_L q_m} \quad (6)$$

Where K_L ($L \cdot mg^{-1}$) is the ratio of the adsorption rate and desorption rate, q_m($mg \cdot g^{-1}$) is the maximum adsorption capacity estimated by the Langmuir model (Langmuir, 1918).

2.6.2.2. Freundlich Isotherm

The Freundlich model is used to represent nonlinear adsorption phenomenon (Freundlich, 1907). It is one of the most widely used isotherms in adsorption. The Freundlich model has been regarded as an empirical equation without physical meaning. In 1947, Halsey and Taylor derived the Freundlich model from the Langmuir isotherm (Zaheer et al., 2019). The linear and nonlinear forms of the Freundlich model is given by the following equations:

$$q_e = K_F C e^{\frac{1}{n}} \quad (7)$$

$$log q_e = log K_F + 1/n log C_e \quad (8)$$

Where K_F ($L^{1/n} \cdot mg^{1-1/n} \cdot g^{-1}$) and n are constants, the Freundlich model will reduce to the linear model when n = 1.

2.6.2.3. Flory Huggins Isotherm

The Flory–Huggins model provides insight into the feasibility and spontaneity of the adsorption process, particularly the degree of surface coverage and the nature of solute–adsorbent interactions. It is given by:

$$q_e = q_m \frac{C}{K_{FH}+C} \quad (9)$$

Where K_{FH} is the Flory–Huggins equilibrium constant and n represent the number of adsorbed molecules occupying a site.

3.0 Results of Characterization of the Functionalized *Bambusa vulgaris* Adsorbent

3.1. Elemental Composition

The elemental composition (C, H, N, and O by difference) of BB and its derivatives functionalized with varying concentrations of ammonia solution (B20 and B30) are presented in Table 1.

Table 1: Elemental Compositions of biochars functionalized with Ammonia (wt%)

Sample	C	H	N	O by diff.	O/C	H/C	(O+N)/C
BB	62.85	1.96	0.85	34.34	0.41	0.37	0.42
B20	58.60	1.96	1.39	38.05	0.49	0.40	0.51
B30	61.78	2.06	1.43	34.73	0.42	0.40	0.44

BB contains 62.85 wt% carbon, 1.96 wt% hydrogen, and 0.85 wt% nitrogen. The comparatively high carbon concentration suggests a high degree of carbonization, as is characteristic of biochars produced at moderate to high pyrolysis temperatures. The high carbon content may indicate that biochar features are hydrophobic, which facilitates adsorption (X. Li et al., 2022). The presence of a trace amount of nitrogen in pristine biochar is due to the nitrogen content of the original bamboo biomass (J. Yang et al., 2021). The oxygen content (by difference) is high, at 34.34 wt%, resulting in an O/C ratio of 0.41. This O/C ratio indicates that the biochar surface has a significant amount of oxygen-containing functional groups, such as hydroxyl, carboxyl, and carbonyl groups, which are known to have a role in adsorption (Park et al., 2019). The H/C ratio of 0.37 shows the degree of aromaticity and carbonization, with lower values generally corresponding to stronger aromaticity (Ranjan et al., 2009).

The functionalization with ammonia solution consistently led to an increase in nitrogen content across the two samples, confirming the successful incorporation of nitrogen onto the biochar surface. In B20, with an increased ammonia concentration, the nitrogen content further rose to 1.39 wt%. The carbon content (58.60 wt%), while the hydrogen content (1.96 wt%) decreased, returning to a level comparable to BB (Z. Zhang et al., 2022). In B30, at the highest ammonia concentration, the nitrogen content reached its peak at 1.43 wt%, representing the most effective nitrogen incorporation

among the ammonia-treated samples. Interestingly, the carbon content (61.78 wt%) increased, approaching that of the pristine biochar, while the oxygen content (34.73 wt%) and O/C ratio (0.42) returned to values very close to the pristine biochar. The hydrogen content (2.06 wt%) and H/C ratio (0.40) also remained relatively stable compared to B20. The (O+N)/C ratio of 0.44 is slightly higher than the pristine biochar, primarily due to the increased nitrogen content. This trend suggests that at higher ammonia concentrations, the treatment might lead to a more stable incorporation of nitrogen with less impact on the overall carbon matrix and oxygen functionalities, possibly due to a more targeted reaction with specific sites on the biochar surface (Peng et al., 2021). The consistent increase in nitrogen content across B20 and B30 confirms the effectiveness of hydrothermal treatment with ammonia solution in introducing nitrogen functional groups. These nitrogen groups, including amine, amide, and pyridinic nitrogen, are known to boost the basicity and electron-donating capabilities of the biochar surface, which are extremely advantageous for the adsorption of anionic dyes like RB5 through electrostatic attraction and hydrogen bonding (B. Li et al., 2018).

3.2 Surface Functional Groups

Fourier Transform Infrared (FTIR) spectroscopy was used to identify and characterize the surface functional groups on BB, B20, and B30. The FTIR spectra, presented in Figure 2 provide crucial insights into the chemical changes induced by the ammonia treatment and confirm the successful incorporation of nitrogen-containing functionalities. A broad band at 3400 cm^{-1} is attributed to the stretching vibrations of O-H groups, which indicate the presence of hydroxyl groups from cellulose, hemicellulose, lignin, and adsorbed water. (Mohan et al., 2006). The peak at 2920 cm^{-1} represents the C-H stretching vibrations of aliphatic groups. A significant peak at approximately 1600 cm^{-1} is typically assigned to the C=C stretching vibrations in aromatic rings, as well as the C=O stretching of carboxyl or carbonyl groups (Yakout, 2017). Bands between 1000 and 1200 cm^{-1} indicate C-O stretching in alcohols, phenols, and ethers. These functional groups add to the overall polarity and adsorption capability of the pure biochar (Y. Li et al., 2014) (Ahmad et al., 2013).

Significant modifications were seen in the FTIR spectra of B20, and B30 after functionalization with an ammonia solution, particularly in regions associated with nitrogen and oxygen functionalities. A key indicator of successful ammonia functionalization is the appearance or enhancement of bands related to nitrogen-containing groups. While a distinct N-H stretching band (typically around 3300 cm^{-1} or 1600 cm^{-1} for primary/secondary amines) might overlap with the O-H or C=C bands, the overall broadening and intensity changes in these regions suggest the presence of N-H bonds. Specifically, the higher intensity of the band about 1600 cm^{-1} in B20, and B30 compared to BB can be attributed not only to C=C and C=O,

but also to N-H bending vibrations of primary amines or C=N stretching from imines (Sekhon & Park, 2021). The increase in nitrogen content, as confirmed by elemental analysis, supports the formation of these groups. The O-H stretching band at 3400 cm^{-1} generally persists across all ammonia-treated samples, indicating that hydroxyl groups are still present, though their exact nature might change due to interactions with nitrogen groups. The intensity of peaks related to C-O stretching around1000-1200 cm^{-1} show variations, suggesting alterations in the oxygen-containing functional groups during the hydrothermal ammonia treatment. Some studies indicate that ammonia treatment can lead to the removal of some oxygen-containing groups or their conversion into nitrogen-containing functionalities (X. Zhang et al., 2014). The positions of characteristic absorption peaks of functional groups were provided in Table 2.

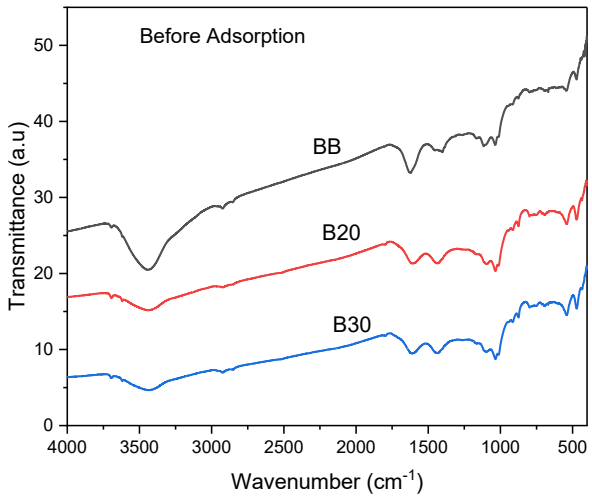


Figure 2: FTIR spectra of BB, B20 and B30

Table 2: Main Functional Groups Present in Biochar

Sample			BB	B20	B30
Wavenumber (cm^{-1})	Functional groups	Compounds			
3200−3700	OH stretching	Aliphatic, aromatic	3445	3439	3435
2700−3000	C-H_n stretching	aliphatic	2937	2919	2920
700-900	C-H	Aromatic hydrogen	842	826	829
1450−1600	C=O	carbonyl	1616	1630	1629
1200−1300	C-O stretching	aryl-alkyl ether linkage, phenol	1220	-	-
700-400	C-C	-	540	546	540

3.3 Thermal Stability

Thermogravimetric Analysis (TGA) was used to assess the thermal stability and degradation behavior of BB, B20 and B30. The TGA curves in Figure 3 show the weight loss of each sample as the temperature increases, providing information about their composition and thermal robustness. The TGA curves often indicate three major stages of weight loss, which corresponds to the normal thermal degradation profile of biomass-derived carbon compounds. The first step of degradation below 150°C revealed that all samples lost a small amount of weight initially. This is mostly caused by the evaporation of physically adsorbed moisture and loosely bound volatile chemicals from the biochar surface (Elnour et al., 2019).

BB shows a relatively lower initial weight compared to the functionalized samples, which might suggest that the ammonia treatment introduces some hydrophilic groups or increases the surface area, leading to higher moisture adsorption. The second stage of degradation (around 150°C to 450-550°C) is the most significant weight loss region for all samples, corresponding to the decomposition of more labile organic components, such as residual hemicellulose and cellulose, and the degradation of some oxygen-containing functional groups such as carboxyl, carbonyl, and hydroxyl groups which are less stable at higher temperatures (Antal & Grønli, 2003). BB shows a sharp drop in weight in this region, indicating the decomposition of its inherent organic matter. B20 and B30 generally exhibit a similar degradation pattern but with slight variations. For instance, B20 appear to show a more pronounced weight loss in the earlier part of this stage compared to BB, which could be related to the decomposition of newly formed nitrogen-containing functional groups or changes in the biochar matrix due to functionalization. The thermal stability of these nitrogen functionalities can vary depending on their chemical (Zaman et al., 2025). The third stage of degradation was observed around 550°C to 1000°C where weight loss becomes more gradual, indicating the decomposition of more recalcitrant carbon structures and the further carbonization of the material. The remaining weight at 1000°C represents the stable carbonaceous char. Notably, B20 and B30 tend to have a higher residual weight percentage at 1000°C compared to BB. This suggests that the ammonia functionalization process may enhance the thermal stability of the biochar matrix, possibly by promoting cross-linking or forming more stable carbon-nitrogen structures (Tang et al., 2025). The formation of stable nitrogen-containing heterocyclic structures within the carbon matrix can enhance the overall thermal resistance of the biochar (Lehmann & Joseph, 2015).

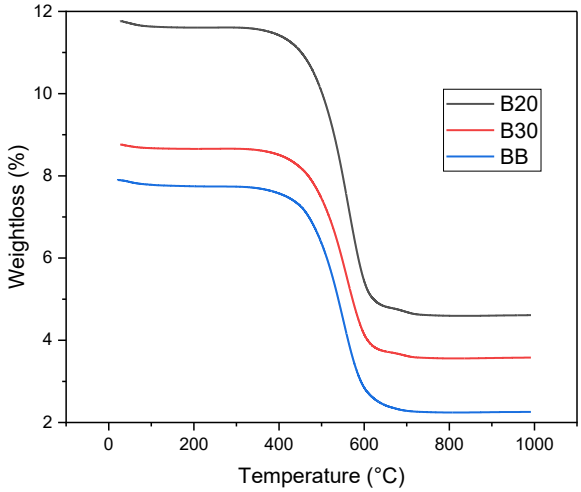


Figure 3 :TGA curves of BB, B20 and B30

3.4. Crystallinity Analysis

X-ray Diffraction (XRD) is a powerful non-destructive analytical technique used to determine the crystallographic structure, phase composition, and crystallite size of materials (S. Chen, 2020; Das et al., 2014). The XRD patterns of BB, B20 and B30 are presented in Figure 4. The XRD pattern of BB typically displays two broad diffraction peaks. The first broad peak, centered around $2\theta \approx 26^0$, corresponds to the (002) plane of graphitic or turbostratic carbon, characteristic of the stacking of aromatic carbon layers (Yakout, 2017). The broadness of this peak indicates a low degree of graphitization and a highly amorphous or disordered carbon structure, which is common for biochars produced at moderate pyrolysis temperatures. The second broad peak, less prominent, typically appears around $2\theta \approx 43^0$, corresponding to the (100) plane, which is related to the in-plane structure of graphitic carbon (Park et al., 2019). The absence of sharp, intense peaks suggests that the pristine biochar is predominantly amorphous with limited long-range crystalline order (Ge et al., 2023).

The XRD patterns of B20 and B30 show similar broad peaks to BB, indicating that the fundamental amorphous carbon structure is largely retained after functionalization. The (002) peak at approximately $2\theta \approx 26^0$ and the (100) peak at $2\theta \approx 43°$ are still present, maintaining their broad nature. This suggests that the hydrothermal ammonia treatment does not significantly alter the overall crystallinity or promote a high degree of graphitization in the biochar matrix (X. Zhang et al., 2014). The functionalization primarily modifies the surface chemistry rather than the bulk crystalline structure. While the main carbon peaks remain broad, subtle changes in their intensity or position might be observed, which could indicate minor structural rearrangements or the incorporation of nitrogen atoms into the carbon lattice. However, no new sharp peaks are observed,

confirming that the ammonia treatment does not lead to the formation of new crystalline inorganic phases. This is consistent with the nature of ammonia functionalization, which primarily involves surface modification and nitrogen doping of the carbon framework (Tomasz Jóźwiak et al., 2022).

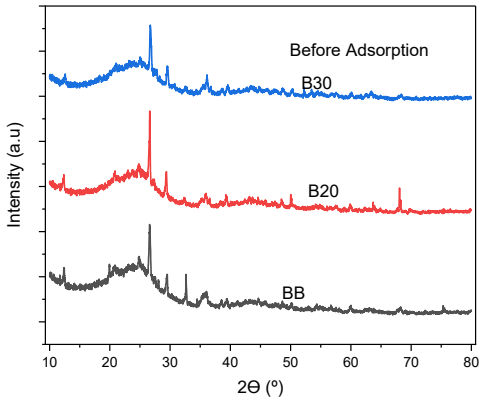


Figure 4: XRD patterns of BB, B20 and B30

3.5. Morphological Analysis

Scanning Electron Microscopy (SEM) is a powerful and necessary technique for characterizing the surface structures and textural features of carbon-based adsorbents (Danya et al., 2024). The SEM images of BB, B20, B30 are presented in Figure 5. The SEM image of BB typically shows a relatively smooth, somewhat fractured, and irregular surface with some visible pores and channels inherited from the original bamboo biomass structure. The surface may appear relatively dense with fewer well-defined pores at this magnification, characteristic of biochar produced at moderate pyrolysis temperatures (Yakout, 2017). Upon functionalization with ammonia solution, indicating successful surface modification. B20 and B30 exhibit a rougher and more irregular surface morphology compared to BB. This increased roughness is indicative of etching effects or the formation of new surface features during the hydrothermal treatment. The images show an increase in the number and accessibility of pores, which is essential for increasing surface area and providing more active sites for dye adsorption (Tomasz Jóźwiak et al., 2022). The functionalization appears to lead to the development of a more heterogeneous pore structure, with evidence of both micropores and mesopores becoming more pronounced. This enhanced porosity is highly beneficial for the adsorption process, as it facilitates the diffusion of dye molecules into the biochar matrix (X. Zhang et al., 2014).

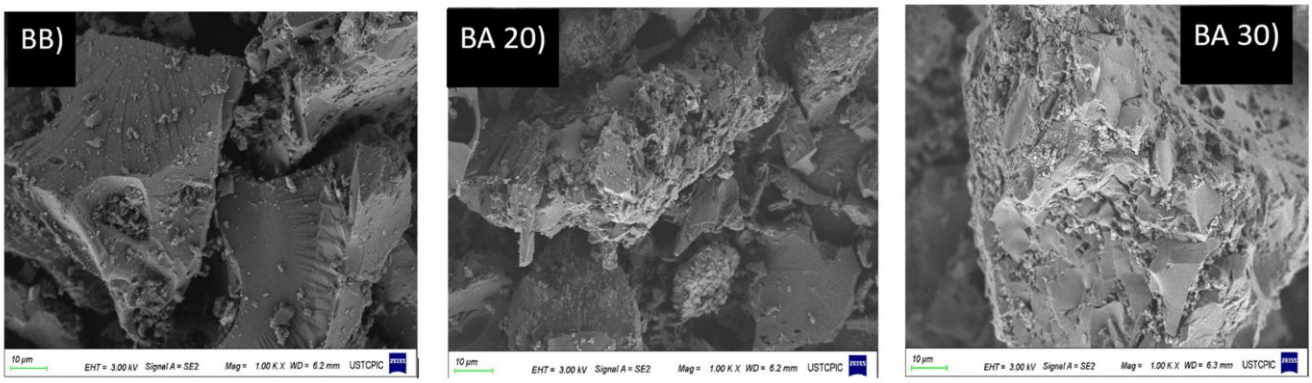


Figure 5:SEM Images of BB, B20 and B30

3.6. Surface Area and Porosity Analysis

The surface area and pore properties of pure and functionalized *Bambusa vulgaris* biochar samples were investigated using nitrogen adsorption-desorption isotherms at 77 K (Z. Liu & Zhang, 2011). The BET surface area, total pore volume, and mean pore diameter for the pristine *Bambusa vulgaris* biochar (BB) and the biochars functionalized with varying concentrations of ammonia solution (B10, B20, B30) are presented in Table 3. Additionally, their nitrogen adsorption-desorption isotherms and pore size distributions are shown in Figure 6a and 6b respectively

BB has a BET surface area of 47.887 m^2g^{-1}, a total pore volume of 0.042 cm^3g^{-1}, and an average pore diameter of 3.473 nm. Its isotherm (figure 6a) often shows a Type II or Type IV isotherm with an H_3 or H_5 hysteresis loop, characteristic of mesoporous materials with slit-shaped pores, which are frequent in biochars generated from lignocellulosic biomass (C. Zhang et al., 2018). The pore size distribution (Figure 6b) indicates the existence of micropores and mesopores. The ammonia functionalization significantly influenced the surface area and pore characteristics, with varying effects depending on the ammonia concentration. B20 exhibits a remarkable increase in BET surface area to 73.134 m^2g^{-1} making it the highest among the ammonia−functionalized samples. The total pore volume also significantly increased to 0.060 cm^3g^{-1}. The mean pore diameter, however, decreased to 3.298 nm, becoming slightly smaller than that of BB. The isotherm for B20 shows a higher nitrogen uptake, especially at higher relative pressures, indicating a more developed mesoporous structure. The pore size distribution for B20 likely shows a more prominent peak in the mesopore range, suggesting that 20 ml of ammonia solution is optimal for creating a highly porous structure with increased accessible surface area. This enhancement is attributed to the etching effect of ammonia during hydrothermal treatment, which can widen existing pores and create new ones (Tomasz Jóźwiak et al., 2022) (X. Zhang et al., 2014). At the maximum ammonia concentration (B30), the BET surface area declined to 43.329 m^2g^{-1}, and the total pore volume was 0.044 cm^3g^{-1}, which was lower than B20 but comparable to or slightly lower

than virgin biochar. The average pore diameter increased to 4.043 nm. This loss in surface area and pore volume at higher ammonia concentrations compared to B20 may be due to severe etching resulting in pore collapse or the agglomeration of biochar particles, which might reduce the accessible surface area (X. Zhang et al., 2014).

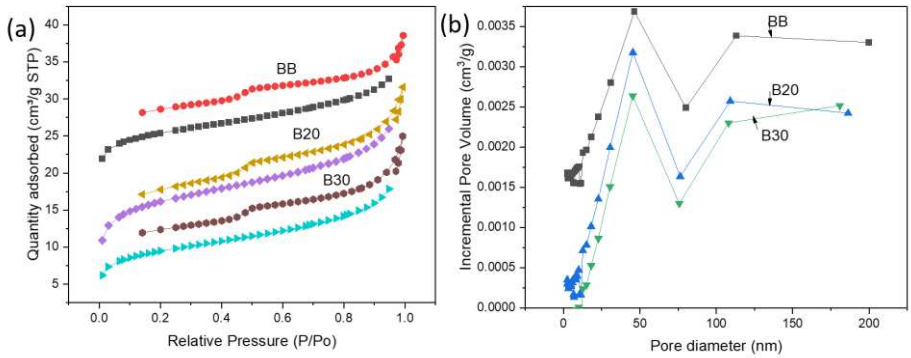


Figure 6(a): Nitrogen adsorption-desorption isotherms (b) Pore size distribution of BB, B20 and B30

Table 3: BET Surface area and pore characteristics of biochar samples.

Biochar Sample	BET Surface Area (m^2g^{-1})	Total Pore Volume (cm^3g^{-1})	Mean Pore Diameter (nm)
BB	47.887	0.042	3.473
B20	73.134	0.060	3.298
B30	43.329	0.044	4.043

3.7. Surface Chemical State

X-ray Photoelectron Spectroscopy (XPS) is a highly surface-sensitive quantitative spectroscopic technique used to detect the elemental composition, chemical states, and electronic states of elements present in the material's topmost layers (usually 1-10 nm). (Oswald, 2006). The XPS derived elemental compositions (%) of BB, B20 and B30 are presented in Table 4. Additionally, the peak binding energies (eV) for C1s, O1s, and N1s are provided in Table 5 and their high-resolution spectra are shown in Figure 7.

BB shows a surface carbon content of 77.06%, oxygen of 21.08%, and nitrogen of 0.92%. The nitrogen content is consistent with the bulk elemental analysis (CHN) and is attributed to the inherent nitrogen in the biomass. The high carbon content indicates a graphitic or carbonaceous backbone, while oxygen signifies the presence of various oxygen-containing functional groups on the surface. All ammonia-functionalized samples exhibit a significant increase in surface nitrogen content compared to BB. B20 has 1.90% N, and B30 has the highest at 2.01% N. This clearly confirms the successful

incorporation of nitrogen onto the biochar surface via the hydrothermal ammonia treatment. The carbon content remains similar to BB for B20 (77.28%) and B30 (77.27%). The oxygen content decreases for B20 (19.79%) and B30 (19.50%), suggesting complex surface reactions involving oxygen-containing groups during functionalization (Hossain et al., 2020).

The C1s spectra for all samples are dominated by a main peak at approximately 284.8 eV, corresponding to graphitic or sp2 hybridized carbon (C-C/C=C) in the biochar backbone (Gürtekin, 2022; Ndoun et al., 2023). Minor peaks or shoulders at higher binding energies (e.g., 285.5-286.5 eV for C-O, 287-288 eV for C=O, and 289 eV for O-C=O) are also present, indicating the presence of various oxygen-containing carbon functionalities. The ammonia functionalization does not significantly shift the main C-C/C=C peak, suggesting the integrity of the carbon framework is maintained. However, subtle changes in the intensity of oxygenated carbon peaks might occur, reflecting surface modifications. The O1s spectra typically show a main peak around 532-533 eV, primarily attributed to C=O (carbonyl/quinone) and C-O (hydroxyl/ether) groups (Goswami et al., 2022). For the ammonia-functionalized samples, the O1s peak generally shifts to slightly lower binding energies (e.g., from 532.95 eV for BB to 532.66 eV for B10, 532.57 eV for B20, and 532.51 eV for B30). This shift, along with changes in peak shape, can indicate alterations in the chemical environment of oxygen due to interactions with nitrogen or a reduction in certain oxygen functionalities. The N1s spectra are crucial for identifying the types of nitrogen functionalities incorporated. For the pristine biochar (BB), the N1s peak at 400.56 eV is likely due to residual nitrogen in the biomass, possibly in the form of pyrrolic or graphitic nitrogen (Zhu et al., 2020). For B20, B30, the N1s peak intensity significantly increases, confirming higher nitrogen content. The N1s spectra can be deconvoluted into various peaks corresponding to different nitrogen species. The shift in the main N1s peak for B20 (400.04 eV) and B30 (400.09 eV) towards lower binding energies compared to BB suggests a change in the dominant nitrogen species, likely indicating an increase in pyrrolic and/or pyridinic nitrogen, which are known to enhance the basicity and electron-donating properties of the biochar surface (Atzei et al., 2014).

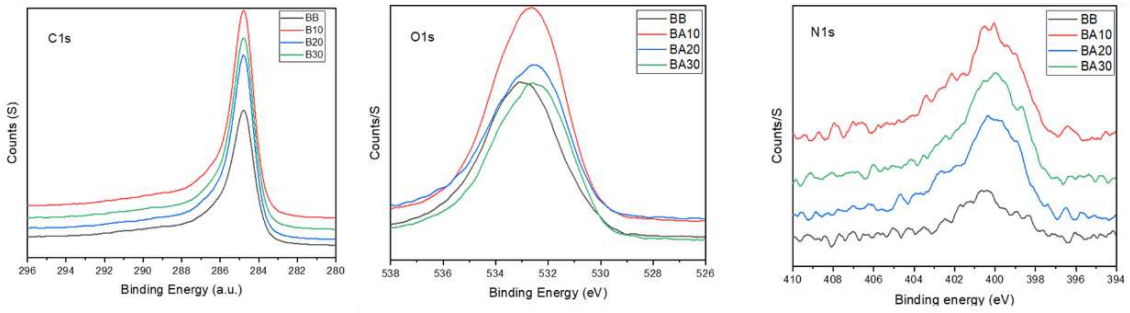


Figure 7: Binding energy analysis of C1s, O1s and N1s of BB, B20 and B30 by XPS

Table 4: XPS derived element composition (%) of the biochars

Sample	C1s	O1s	N1s
BB	77.06	21.08	0.92
B20	77.28	19.79	1.90
B30	77.27	19.5	2.01

Table 5: XPS derived peak binding energy (eV) of the biochars

Sample	C1s	O1s	N1s
BB	284.8	532.95	400.56
B20	284.8	532.57	400.04
B30	284.8	532.51	400.09

4. Adsorption Test

4.1 Effect of Initial Concentration

A comprehensive comparative analysis of the effect of initial dye concentration on the adsorption capacity of RB5 dye across the pristine *Bambusa vulgaris* biochar (BB) and the ammonia-functionalized biochars (B20 and B30) (figure 8) reveals distinct performance enhancements due to functionalization. All three adsorbents (BB, B20, B30) consistently demonstrated an increase in adsorption capacity as the initial dye concentration increased from 3 ppm to 30 ppm. Both B20 and B30 exhibited substantially higher adsorption capacities compared to BB across the entire range of initial dye concentrations. At lower starting concentrations, adsorption capacity rose dramatically. This quick growth is owing to the high number of unoccupied active sites on the biochar surface in comparison to the amount of dye molecules (Zhao et al., 2024). The large concentration gradient serves as a powerful driving force, promoting the effective transfer of dye molecules from the solution to the adsorbent surface (Goswami et al., 2022). As the initial dye concentration increased from 12 ppm to 30 ppm, the rate of increase in adsorption capacity decreased slower. This phenomenon normally occurs once the adsorption sites on the biochar surface become saturated. At increased dye concentrations, competition for the remaining active sites rises, and the driving force for adsorption decreases (Zhao et al., 2024). The maximum adsorption capacity was found at an initial concentration of 30 ppm, indicating that there were more dye molecules accessible to interact with the biochar surface. This trend is consistent with conventional adsorption processes, where increasing the initial adsorbate concentration leads to greater adsorption capabilities until saturation is achieved (Gupta & Bhattacharyya, 2011; Xue et al., 2009). This enhanced efficacy is primarily due to the effective integration of nitrogen-containing functional groups into their surfaces after ammonia treatment. Elemental analysis and XPS reveal that these basic nitrogen groups considerably enhance the number of

active sites accessible for electrostatic interaction with the Reactive Black 5 dye's anionic sulfonate groups. The functionalized surfaces' higher polarity and hydrophilicity contribute to greater interaction with the dye in aqueous solution (Tomasz Jóźwiak et al., 2022).

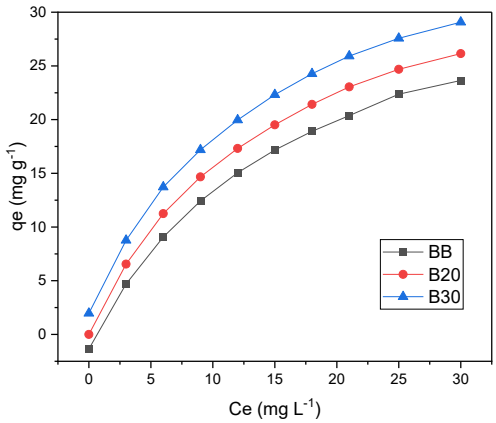


Figure 8:Effect of initial dye concentration on the adsorption capacity of RB5 by BB, B20 and B30

4.2 Effect of Contact Time

The time required for an adsorbent to reach equilibrium is critical for adsorbent selection because the goal is to get the highest adsorption efficiency in the shortest amount of time. If an adsorbent takes a long time to reach equilibrium, regeneration will be time-consuming, which is not cost-effective for practical applications. The higher the reaction rate, the shorter the equilibrium time (Uddin et al., 2021). A comparative analysis of the effect of contact time across BB, B20 and B30 is illustrated in Figure 9. All three adsorbents exhibited the characteristic two-phase adsorption process i.e rapid initial uptake followed by a slower attainment of equilibrium. Both B20 and B30 consistently demonstrated higher adsorption capacities and generally faster equilibrium times compared to BB. This enhancement is mostly owing to increased availability of active sites and improved textural qualities as a result of functionalization (Al-dhawi et al., 2023). Among the ammonia-functionalized samples, B20 consistently showed superior performance in terms of both adsorption rate and capacity. This is likely due to its optimal balance of nitrogen incorporation and surface area development, as indicated by previous characterization analyses (Sing, 2001) (Guo et al., 2023).

While B30 also improved over BB, its performance was slightly less than B20. This suggests that the 20ml ammonia concentration provided the most favorable conditions for creating an efficient adsorbent for RB5 dye under the tested contact time range. The observed equilibrium time of approximately 120 minutes was generally consistent across all three

adsorbents, indicating this duration is sufficient for the adsorption process to reach a steady state under the experimental conditions (Murphy et al., 2023) (X.-Y. Yang & Al-Duri, 2001).

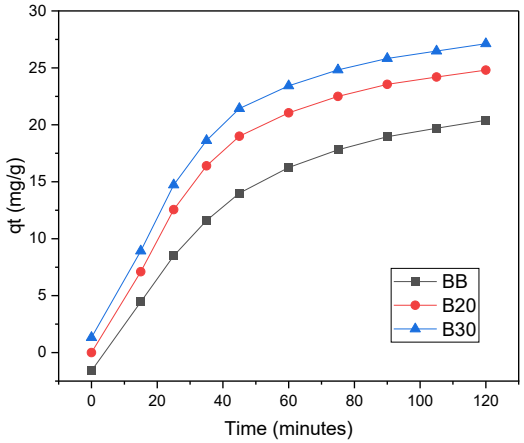


Figure 9: Comparative effect of contact time on the adsorption capacity of RB5 dye by BB and B20 and B30

4.3. Effect of Solution pH

One of the most critical parameters influencing adsorbent capacity in wastewater treatment is solution pH. The efficacy of adsorption is reliant on the solution pH, because difference in pH leads to variations in the degree of ionization of the adsorptive molecule and the surface characteristics of the adsorbed substance (Al-Degs et al., 2008). The effect of solution pH on the adsorption capacity of Reactive Black 5 (RB5) dye by BB, B20 and B30 is presented in Figure 10. The pH of the dye solutions was varied from 1 to 9. The adsorption capacity of RB5 dye onto all three biochar samples (BB, B20, and B30) was significantly influenced by the solution pH, exhibiting a clear trend that can be explained by the surface charge of the adsorbents and the anionic nature of the dye. For all three biochars, the adsorption capacity was highest at acidic pH values, particularly at pH 3. The adsorption capacity of BB was highest at pH 3, and then decreased as pH increased. At low pH, the biochar surface becomes protonated due to the abundance of H^+ ions, leading to a positively charged surface (e.g., $-OH^-$). This positively charged surface strongly attracts the negatively charged sulfonate groups of the anionic RB5 dye through electrostatic interactions (Mahbub et al., 2019). B20 and B30 also showed their highest adsorption capacities at pH 3. Infact, they exhibited superior adsorption capacities compared to BB at this pH. This is a direct consequence of the successful incorporation of basic nitrogen-containing functional groups during ammonia functionalization, as confirmed by elemental analysis and XPS (Arrigo et al., 2010). These nitrogen groups are readily protonated in acidic environments, significantly increasing the positive charge density on the biochar surface and thus enhancing the electrostatic attraction with the anionic

RB5 dye. Between B20 and B30, B20 generally showed a slightly higher adsorption capacity at pH 3, consistent with its optimal surface area and nitrogen functionalization balance. As the solution pH increased from acidic to neutral and then alkaline conditions, the adsorption capacity for all biochars significantly decreased. At higher pH values, the concentration of H^+ ions decreases, leading to deprotonation of the biochar's surface functional groups. This results in a more negatively charged or neutral surface (Z. Tan et al., 2020). For the anionic RB5 dye, as the pH increases, the repulsive forces between the negatively charged dye molecules and the increasingly negatively charged biochar surface intensify, leading to a reduction in adsorption capacity (Xie et al., 2021).

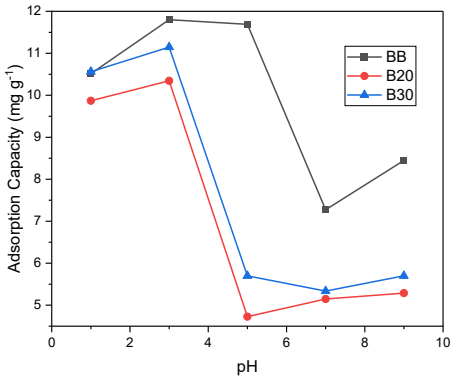


Figure 10: Effect of solution pH on the adsorption capacity of RB5 dye BB, B20 and B30

4.4. Effect of Adsorbent Dose

Adsorbent dose is an important process parameter for determining an adsorbent's capacity for a given amount of adsorbent under operating conditions. The amount of adsorbent used is an important factor in determining removal efficiency. In general, increasing the amount of adsorbent resulted in tangibly larger clearance percentages because bigger doses of adsorbent provide more binding sites for RB5 adsorption. However, utilizing significant volumes of adsorbent is not recommended due to economic considerations. In this regard, producing adsorbents with larger binding sites, specific surface area, porosity, and consequently enhanced adsorption capacity is very important (Crini & Badot, 2008). The effect of adsorbent dose on the adsorption capacity of RB5 dye by BB, B20 and B30 is presented in Figure 11. The adsorbent dosage was varied from 0.04 g to 1.0 g. The adsorption capacity of RB5 dye onto all three biochar samples consistently decreased with an increase in adsorbent dose, while the overall percentage removal efficiency would typically increase. For all adsorbents, the adsorption capacity showed a sharp decline as the adsorbent dose increased from 0.04 g to 1.0 g. Additionally, at higher adsorbent doses, phenomena such as site overlapping or aggregation of adsorbent particles can occur. This can

reduce the effective surface area available for adsorption and increase the diffusion path length for dye molecules, leading to a less efficient utilization of all available sites (Hadi et al., 2015).

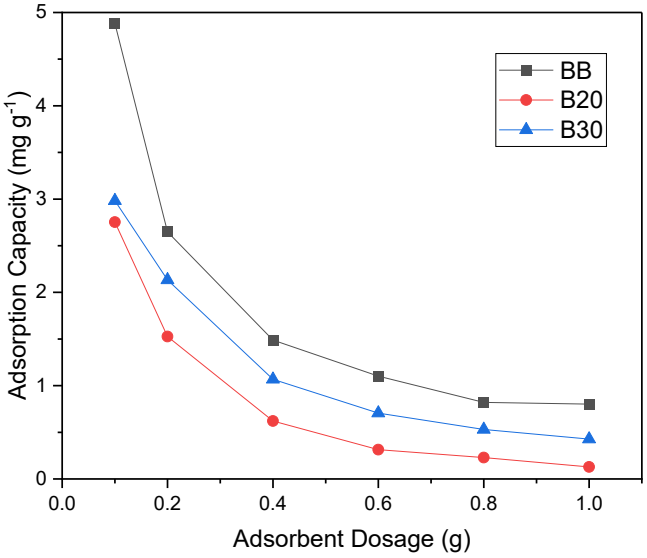


Figure 11:Effect of Adsorbent Dosage on the adsorption capacity of RB5 dye on BB, B20 and B30

4.5 Adsorption Kinetics

The adsorption kinetics of RB5 dye onto BB, B20 and B30 using three kinetic models: the Pseudo First-Order (PFO), Elovich, and Intraparticle Diffusion models is shown in figure 12. These models were employed to elucidate the mechanisms governing the dye uptake, determine the adsorption rate, and evaluate whether the process was controlled by surface interactions or internal diffusion. Among the models investigated, the Pseudo First-Order (PFO) model exhibited the best fit to the experimental data, as evidenced by the highest correlation coefficients (R^2) for all three biochar samples (table 6). Specifically, BB had an R^2 value of 0.99792, followed by B20 (0.99446) and B30 (0.9942), indicating that the PFO model effectively described the adsorption behavior. This suggests that the rate of dye uptake was primarily controlled by physisorption mechanisms, where the adsorption rate is proportional to the number of available sites on the adsorbent surface (Y.-S. Ho & Mckay, 1998). The calculated equilibrium adsorption capacities (q_e) increased with ammonia treatment, with B30 recording the highest value of 26.83 mg/g, followed by B20 (25.97 mg/g) and BB (23.60 mg/g). This trend suggests that the chemical treatment enhanced the adsorptive affinity of the biochars, likely due to increased surface functional groups and modified surface chemistry.

The Elovich model, often used to describe chemisorption on heterogeneous surfaces (Chien & Clayton, 1980), also fitted the data well but with slightly lower R^2 values (BB= 0.98866, B20=0.97882, B30=0.97736). The initial adsorption rate

(α) increased from 0.74819 mg/g·min for BB to 1.06073 and 1.17754 mg/g·min for B20 and B30, respectively, indicating enhanced surface reactivity due to ammonia modification. However, the β parameter (indicating the extent of surface coverage) remained relatively consistent across all samples, suggesting that the modification primarily affected the surface energy rather than surface uniformity. While the Elovich model supports the presence of chemisorptive interactions, the overall fit indicates that chemisorption may play a supplementary role rather than being the dominant mechanism.

The Intraparticle Diffusion model was applied to explore the diffusion of RB5 molecules within the internal pores of the biochars. The model showed good linearity with R^2 values of 0.97489 for BB, 0.9759 for B20, and 0.9389 for B30. These values, although slightly lower than those of the PFO model, suggest that intraparticle diffusion is a significant but not exclusive rate-limiting step. The rate constants (k_{id} increased from 2.16421 mg/g·min for BB to 2.42922 for B20 and 2.51417 for B30, further confirming that ammonia treatment enhanced internal diffusion, possibly due to improved porosity and reduced pore blockage. Additionally, the intercept values (C), which relate to boundary layer thickness, also increased in the order BB (0.23966) < B20 (0.45255) < B30 (0.69987). These increasing C values indicate the presence of an external film diffusion step and suggest a more pronounced boundary layer resistance in the treated biochars, likely due to the enhanced surface interactions with RB5.

Table 6: Parameters of Non-Linear Pseudo first order fitting, Elovich model and intraparticle Diffusion for RB5 Adsorption

Adsorbent	**PFO**			**Elovich**			**Intraparticle Diffusion**		
	R^2	K_1	qe	R^2	α	β	R^2	k_{id}	C
BB	0.99792	0.02288	23.60218	0.98866	0.74819	0.10052	0.97489	2.16421	0.23966
B20	0.99446	0.02692	25.97075	0.97882	1.06073	0.10049	0.95759	2.42922	0.45255
B30	0.9942	0.02803	26.83	0.97736	1.17754	0.10003	0.95389	2.51417	0.69987

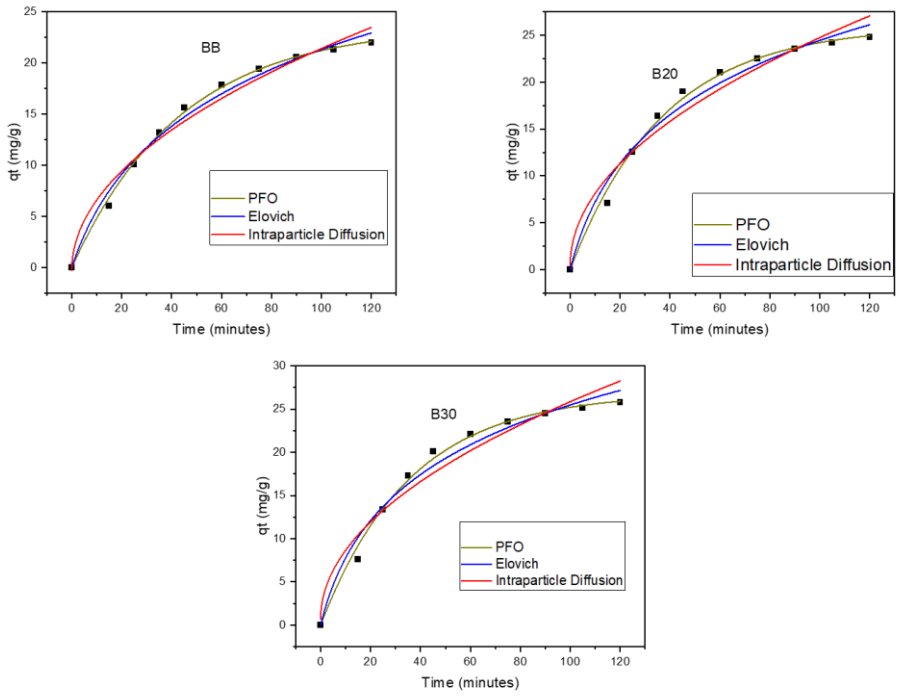


Figure 12: Adsorption Kinetics for BB and biochars functionalized with Ammonia

4.6 Adsorption Isotherms

To gain insights into the adsorption behavior and interaction mechanisms of RB5 dye on biochars, three commonly used isotherm models: Langmuir, Freundlich, and Flory Huggins were applied to the equilibrium data (figure 13). The Langmuir model fitted the data with exceptionally high R^2 values: BB (0.99983), B20 (0.9999), and B30 (0.99989), confirming its suitability and implying that RB5 adsorption was likely monolayer in nature on uniform active sites of the adsorbents. The maximum adsorption capacity q_{max} increased slightly with modification: BB (38.81 mg/g), B20 (39.58 mg/g), and B30 (40.91 mg/g). This trend indicates that ammonia treatment enhanced the surface functionality and created more accessible adsorption sites, thereby improving the uptake potential. The Langmuir constant K_L, which indicates the affinity of the dye molecules to the surface, also showed a slight increase from BB (0.0611 L/mg) to B20 (0.06554 L/mg) and B30 (0.06632 L/mg), further supporting the enhanced binding affinity after modification. The outstanding R^2 values reinforce that Langmuir best describes the equilibrium adsorption for all samples, consistent with other dye-biochar studies (Goswami et al., 2022).

The R^2 values were also high for the Freundlich model but lower than Langmuir: BB (0.99248), B20 (0.99217), and B30 (0.9917). These values still indicate a good fit, suggesting the presence of heterogeneous surface energies on the biochar

surfaces, particularly after modification. The K_F values increased progressively from BB (4.04106) to B20 (4.44448) and B30 (4.649), suggesting improved adsorption strength and surface activity due to the introduction of nitrogen-containing functional groups via ammonia treatment. The Freundlich exponent n ranged from 1.82 to 1.88 for all samples, which are all greater than 1 implying favorable adsorption and strong interactions between RB5 molecules and the adsorbents (Foo & Hameed, 2010). These values confirm that RB5 adsorption is not only physical but may involve some degree of surface heterogeneity and multilayer adsorption, especially with chemically modified biochars.

The q_{max} values for Flory–Huggins were lower compared to the Langmuir model: BB (0.6726 mg/g), B20 (0.69487 mg/g), and B30 (0.71187 mg/g), suggesting the model may not fully describe the adsorption process quantitatively but rather supports thermodynamic and surface interaction aspects. The values of K_{FH} followed the order BB > B20 > B30, indicating that although all adsorption processes were spontaneous, the spontaneity slightly decreased with increased ammonia treatment. Notably, the values of n remained constant at 1 across all samples, suggesting that a single RB5 molecule interacts with one active site, consistent with Langmuir's monolayer assumption. The fitting parameters were provided in Table 7.

Overall, among the three models tested, Langmuir provided the best fit, highlighting that RB5 adsorption onto BB, B20, and B30 primarily occurred via monolayer coverage on homogeneous sites.

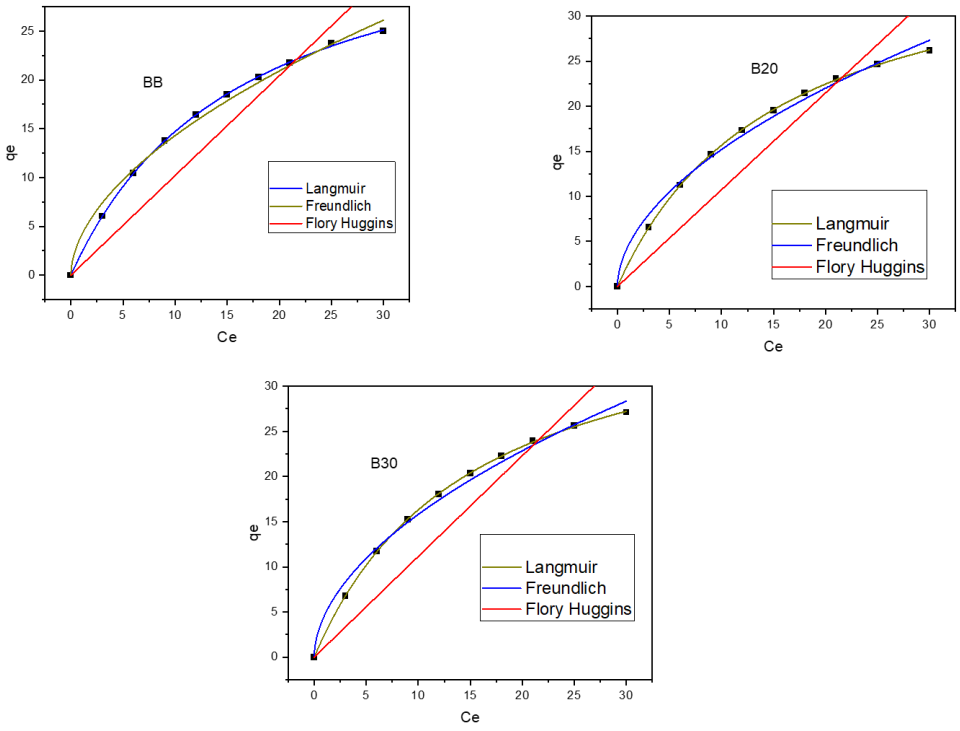


Figure 13: Adsorption Isotherms for BB and biochars functionalized with Ammonia

Table 7: The parameters for non-linear fitting of Langmuir, Freundlich and Flory Huggins Isotherms for adsorption of RB5 by BB, B20 and B30

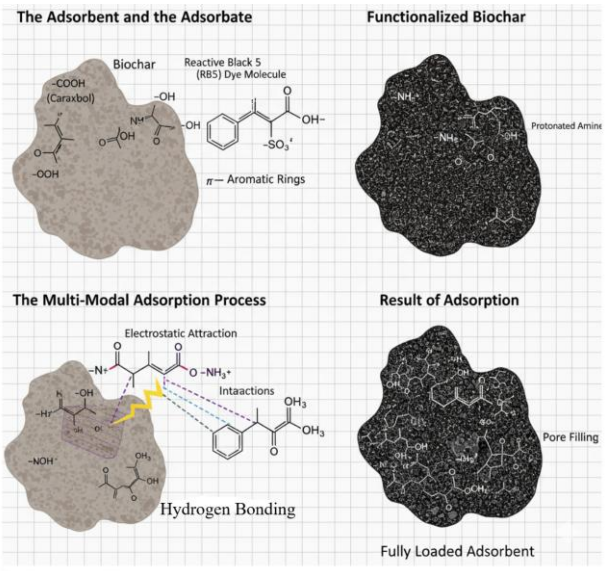
Adsorbent	**Langmuir**			**Freundlich**			**Flory Huggins**			
	R^2	q_{max}	K_L	R^2	K_F	n	R^2	q_{max}	n	K_{FH}
BB	0.99983	38.80538	0.0611	0.99248	4.04106	1.82262	0.80493	0.6726	1	1.93106
B20	0.9999	39.58295	0.06554	0.99217	4.44448	1.87298	0.78619	0.69487	1	1.8331
B30	0.99989	40.90559	0.06632	0.9917	4.649	1.88122	0.78254	0.71187	1	1.76399

4.7 Adsorption Mechanism

The adsorption of RB5 dye onto BB, B20 and B30 is a multi-mechanistic process governed by a combination of physicochemical interactions, which was illustrated schematically in figure 14. Electrostatic attraction is considered a primary driving force for the adsorption of anionic RB5 dye. RB5 is a reactive dye with sulfonate groups ($-SO_3^-$) that render it negatively charged in aqueous solutions across a wide pH range. As demonstrated earlier, the adsorption capacity of all biochars was significantly higher at pH 3. At low pH, the surface of the biochar becomes protonated. Functional groups such as amines ($-NH_2$), imines (=NH), and pyridinic nitrogen on the functionalized biochars acquire a positive charge ($-NH_3^{2+}$,

593 $=NH^{2+}$). This positively charged surface strongly attracts the negatively charged sulfonate groups of RB5 dye through
594 electrostatic forces, leading to enhanced adsorption. As pH increases, the surface charge of the biochar becomes less positive
595 or even negative due to deprotonation of acidic functional groups and deionization of basic groups, increasing electrostatic
596 repulsion with the anionic dye and consequently reducing adsorption (Q. Liu et al., 2021).

597 Hydrogen bonding plays a significant role, particularly between the oxygen-containing functional groups and nitrogen-
598 containing groups on the biochar surface, and the various polar groups such as, -OH, -NH, $-SO_3H$) present in the RB5 dye
599 molecule. FTIR analysis revealed the presence and changes in O-H, C=O, and C-O stretching vibrations in both pristine and
600 functionalized biochars. The introduction of N-H groups via functionalization further provides sites for hydrogen bond
601 formation. Both the biochar and the Reactive Black 5 dye molecule possess extensive π-electron systems. RB5 dye also
602 contains multiple aromatic rings. These parallel aromatic rings can engage in π-π stacking interactions, where the π-electrons
603 of the dye molecules interact with the π-electron clouds of the biochar surface (Sutradhar et al., 2024). This interaction
604 contributes to the adsorption, especially at higher dye concentrations. The porous structure of biochar provides physical sites
605 for dye molecules to be trapped and adsorbed. SEM images confirmed the development of porous structures, and BET
606 analysis quantified the surface area and pore volume of the biochars. The presence of micropores and mesopores allows for
607 the physical entrapment of dye molecules within the adsorbent matrix. The initial rapid adsorption phase observed in contact
608 time studies is largely attributed to the adsorption on the external surface, followed by a slower diffusion into the internal
609 pores (B. Chen et al., 2001). Therefore, the pore filling mechanism is a significant contributor to the overall adsorption
610 capacity, especially for larger dye molecules.



611

Figure 14: Multi-Mechanistic Adsorption Mechanism of RB5 Dye onto Functionalized *Bambusa vulgaris* Biochar

5. Reusability of Adsorbents

The reusability of an adsorbent is a critical factor for its practical and economic viability in wastewater treatment applications (Obodo & Aigbe, 2023). To evaluate this, BB, B20 and B30 were subjected to 8 successive adsorption-desorption cycles. The percentage removal efficiency was monitored for each cycle, and the results are summarized in Table 8 and shown in figure 15. In the first adsorption cycle, B20 and B30 demonstrated significantly higher RB5 dye removal efficiencies (92.5% and 89.8%, respectively) compared to BB, which achieved 75.2% removal. For all three adsorbents, a gradual decrease in removal efficiency was observed over the 8 successive adsorption-desorption cycles. The removal efficiency of BB decreased from 75.2% in the first cycle to 48.5% by the eighth cycle, representing a decline of approximately 35.5% from its initial efficiency. B20 maintained a higher removal efficiency throughout the cycles, dropping from 92.5% to 67.8%. B30's efficiency decreased from 89.8% to 66.2% (a decline of approximately 26.3%). This decline is a common phenomenon in adsorption processes and can be attributed to the fact that some dye molecules may be strongly or irreversibly bound to the active sites, preventing their complete desorption in subsequent regeneration steps.

Despite the observed decline, B20 and B30 consistently maintained significantly higher removal efficiencies throughout all 8 cycles compared to the pristine BB. For instance, even after 8 cycles, B20 and B30 still achieved removal efficiencies of 67.8% and 66.2%, respectively, which are considerably higher than BB's initial performance of 75.2% and its final performance of 48.5%. Also, B20 and B30 showed a more stable performance profile, with a lower percentage decrease from their initial efficiency compared to BB. This indicates that the ammonia functionalization not only enhances the initial adsorption capacity but also contributes to better reusability and long-term stability of the adsorbents. The introduced nitrogen-containing groups likely form more stable interactions with the biochar matrix, making them more resistant to degradation during regeneration (Luo et al., 2023).

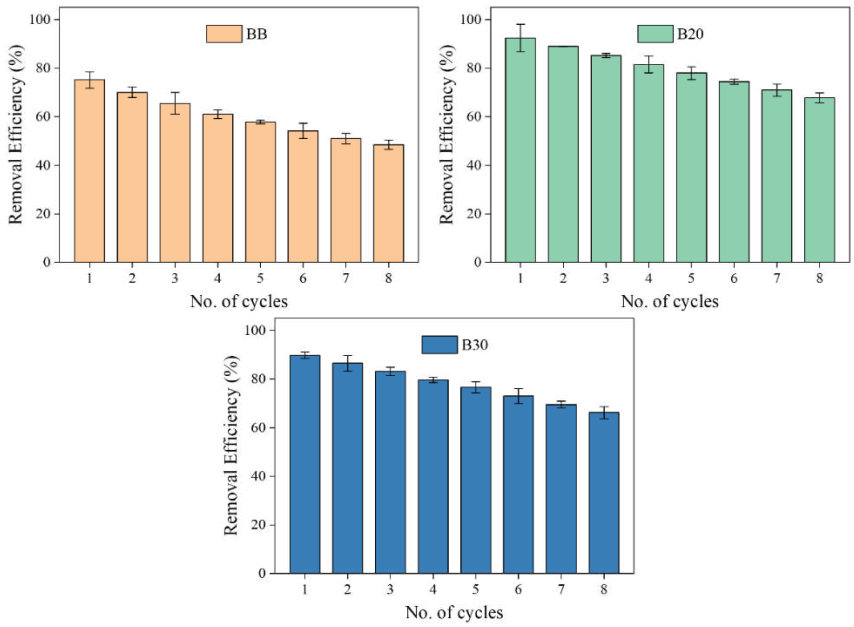


Figure 15: Reusability of BB, B20 and B30

Table 8: Removal Efficiency (%) and number of cycles

Adsorbent	Cycle 1	Cycle 2	Cycle 3	Cycle 4	Cycle 5	Cycle 6	Cycle 7	Cycle 8
BB	75.2	70.1	65.5	61.0	57.8	54.2	51.0	48.5
B20	92.5	89.0	85.2	81.5	78.0	74.5	71.0	67.8
B30	89.8	86.5	83.1	79.7	76.7	73.0	69.5	66.2

5.1 Post-Adsorption Characterization

5.1.1 Elemental Composition

The elemental and atomic ratio analysis of biochars of BB, B20 and B30 were compared before and after adsorption (table 9). For the pristine biochar (BB), the carbon content increased from 62.85% to 67.740%, and hydrogen content slightly increased from 1.96% to 2.224%. This rise in carbon and hydrogen suggests the retention of some organic components from the dye that were not fully desorbed, leading to a higher relative percentage of these elements in the residual material. Conversely, the nitrogen content decreased from 0.85% to 0.650%, and oxygen content reduced from 34.34% to 29.386%. These reductions in nitrogen and oxygen indicate a loss of some inherent functional groups during the 8 cycles of adsorption, which contributes to the observed decline in its reusability. The decreased O/C and (O+N)/C ratios further confirm a reduction in surface polarity and the overall content of oxygen and nitrogen functionalities (X.-F. Tan et al., 2021).

For B20, the carbon content increased from 58.60% to 61.340%, similar to BB, suggesting some dye residue. Hydrogen content showed a minimal decrease from 1.96% to 1.925%, indicating relative stability. However, a significant decrease in nitrogen content was observed, from an initial 1.39% to 0.770% post-adsorption. This substantial loss of nitrogen is a key finding, as it directly indicates that a considerable portion of the nitrogen-containing functional groups, which were crucial for enhancing RB5 adsorption, were either leached or degraded during the repeated cycles. This loss directly explains the observed decrease in reusability for B20. Oxygen content also decreased from 38.05% to 32.965%, suggesting a loss of oxygen-containing functional groups. The reduced O/C and (O+N)/C ratios further reflect a decline in surface polarity and active sites (Kurniawan et al., 2024).

Similarly, for the B30, carbon content increased from 61.78% to 67.380%, likely due to residual dye. Hydrogen content remained relatively stable, changing only slightly from 2.06% to 2.046%. The nitrogen content decreased from 1.43% to 0.940% post-adsorption. While still a significant reduction, it is noteworthy that the final nitrogen content of B30 (0.940%) is higher than that of both BB (0.650%) and B20 (0.770%) after 8 cycles. This suggests that B30 retained a relatively higher proportion of its nitrogen functionalities, which might contribute to its slightly better reusability in the later cycles, as observed in Table 6.2 (S. Wang et al., 2018) where B30's final efficiency is comparable to B20's. Oxygen content also decreased from 34.73% to 29.634%, indicating a loss of oxygen-containing groups. The corresponding decreases in O/C and (O+N)/C ratios reflect the overall loss of these functionalities (L. Wang et al., 2018).

Table 9: Elemental Compositions of the Biochar after Adsorption

Sample	C (%)	H (%)	N (%)	O (%)	O/C	H/C	(O+N)/C
BB	67.740	2.224	0.650	29.386	0.325	0.394	0.333
B20	61.340	1.925	0.770	32.965	0.403	0.377	0.412
B30	67.380	2.046	0.940	29.634	0.330	0.364	0.374

5.1.2. Surface Functional Groups Analysis

Fourier Transform Infrared (FTIR) spectroscopy was performed on the biochar samples (BB, B20, and B30) after adsorption of RB5. The pre and post-adsorption FTIR spectra are presented in Figure 16. For all samples (BB, B20, B30), the post-adsorption spectra show new peaks or increased intensity in regions characteristic of the Reactive Black 5 dye molecule. Specifically, the presence of strong absorption bands around 1100-1200 cm^{-1} and 1000-1050 cm^{-1} can be attributed to the stretching vibrations of the sulfonate groups of RB5 dye (Arslan-Alaton et al., 2023). Other peaks corresponding to C-N, C-O, and aromatic C=C stretching from the dye molecule might also become more pronounced or overlap with existing biochar peaks. This directly confirms the successful adsorption of RB5 dye onto the biochar surfaces. The broad band for O-H

stretching might show a decrease in intensity or a shift, suggesting the involvement of hydroxyl groups in hydrogen bonding with the dye molecules (Ovchinnikov et al., 2016). The region, which includes C=C aromatic stretching and C=O stretching from biochar, might show changes due to the overlap with N-H bending vibrations and C=N stretching from adsorbed dye molecules or altered biochar functionalities. The presence of adsorbed dye could lead to an increase in the intensity of this band. For the functionalized biochars, changes in the N-H bending region or the appearance of new N−H stretching bands around 3300 cm^{-1} could indicate the involvement of amine/amide groups in hydrogen bonding or electrostatic interactions with the dye (Liu et al., 2015). The changes observed in the post-adsorption FTIR spectra provide direct spectroscopic evidence supporting the proposed adsorption mechanisms.

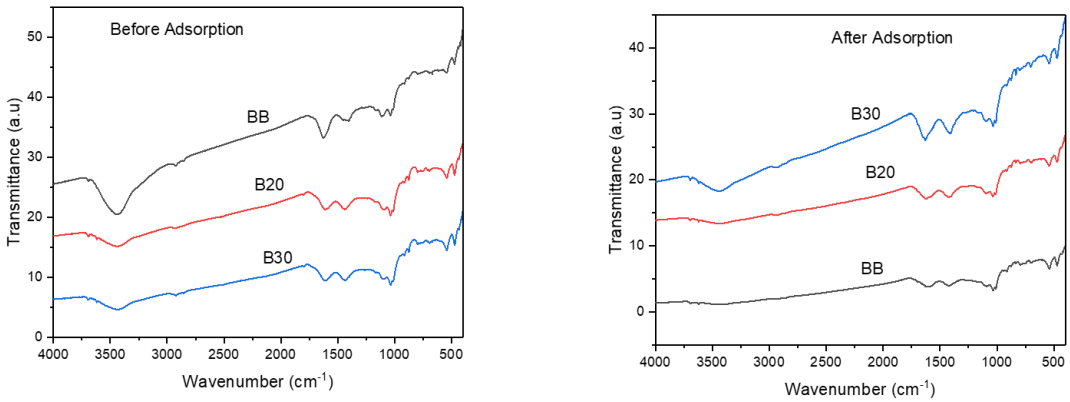


Figure 16: FTIR Spectra of BB, B20 and B30 before and after adsorption

5.1.3. Crystallinity Analysis

The X-ray diffraction (XRD) patterns of BB, B20 and B30 after adsorption are presented in Figure 17. Before adsorption, all samples displayed two major broad peaks within the ranges of 14–30° and 40–45°, corresponding to the (002) and (100) planes of graphitic carbon, respectively. The (002) peak reflects the stacking of aromatic carbon sheets, while the (100) peak is attributed to in-plane ordering within the graphitic structure (Kambo & Dutta, 2015a). The presence of these weak and broad peaks confirmed the predominantly amorphous and disordered nature of the biochar samples, which is favorable for adsorption due to the abundance of surface defects and edge-plane sites that serve as active centers (Mahdi et al., 2019) (Ahmad et al., 2014; Y. Li et al., 2014).

Post-adsorption XRD patterns revealed that this structural disorder was generally retained in all biochars. However, notable differences were observed in the intensity and sharpness of the diffraction peaks among the samples. The untreated BB sample retained its original broad (002) peak around 2θ (22–26°), with minimal changes in intensity, indicating that its

internal carbon structure remained largely unaltered after dye adsorption. This supports the earlier BET and SEM findings that showed limited porosity and adsorption efficiency in BB.

In contrast, the ammonia-modified samples B20 and B30 exhibited sharper and more intense peaks in the same 2θ range, especially for the (002) reflection. This change suggests partial structural reorganization or increased aromatic condensation within the carbon framework due to chemical activation and subsequent adsorption. The enhancement in peak definition for B20, in particular, may be associated with the effective removal of surface impurities and re-alignment of microcrystalline domains following ammonia treatment (Wu et al., 2012). Although B30 also showed sharper peaks compared to BB, its broader baseline implies a higher degree of microstructural disorder, potentially due to excessive ammonia treatment, which could have induced structural degradation or pore-wall collapse. These changes, however, were not significant enough to transform the materials into crystalline phases, confirming that all samples remained within the amorphous regime. The slight increase in crystallinity indicators in B20 and B30 does not contradict their performance as adsorbents, as amorphous carbon structures are often preferred in adsorption applications for their rich surface functionality and accessible active sites (Yin et al., 2017).

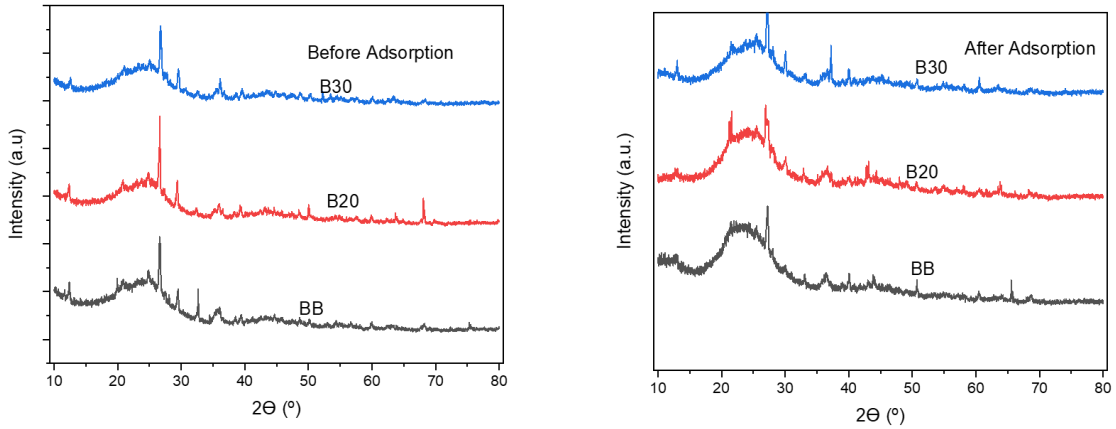


Figure 17: XRD Spectra of BB, B20 and B30 before and after adsorption

5.1.4. Morphological Analysis

Scanning Electron Microscopy (SEM) analysis was performed on the biochar samples (BB, B20, and B30) after adsorption of Reactive Black 5 (RB5) dye. The post-adsorption SEM images are presented in Figure 18. The post-adsorption SEM images generally show changes in the surface morphology of all biochar samples (BB, B20, B30) compared to their pristine states. The surfaces appear less clean and may exhibit a layer or deposits of adsorbed dye molecules. This can manifest as a slight smoothing of previously rough areas or, conversely, the appearance of aggregated dye particles on the

surface, especially at higher dye loadings. For the functionalized biochars (B20 and B30), the images show the dye molecules adhering to the nitrogen-rich sites or filling the pores created during functionalization. While the overall porous structure of the biochars is largely maintained, some degree of pore blockage might be observed, particularly for smaller pores, as dye molecules occupy the available pore space.

Despite the presence of adsorbed dye, the fundamental structural integrity of the biochar particles appears to be largely preserved. There is no clear evidence of significant structural damage or complete collapse of the pore network due to the adsorption process itself. This structural robustness is important for the adsorbent's mechanical stability and reusability. The visual evidence of dye deposition on the biochar surfaces in the post-adsorption SEM images directly confirms the successful adsorption of Reactive Black 5 dye. The extent of surface coverage and the nature of the deposits can also provide qualitative insights into the adsorption capacity and the distribution of adsorbed dye molecules (Z. Li et al., 2020).

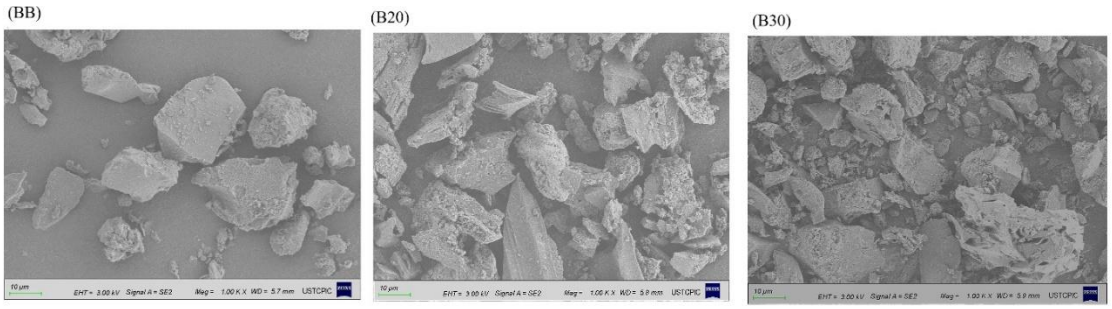


Figure 18: SEM Images of BB, B20, and B30 after Adsorption

5.1.5 Surface Area and Porosity Analysis

The BET surface area, total pore volume, and mean pore diameter are essential parameters in evaluating the textural characteristics of porous materials, especially for adsorption applications. These parameters were measured for BB, B20 and B30 after adsorption. The results are presented in the table 10 below and are further supported by the nitrogen adsorption-desorption isotherms and pore size distribution plots (figure 19).

Before adsorption, the BET analysis showed that B20 had the highest surface area (73.134 m^2/g), followed by BB (47.887 m^2/g) and B30 (43.329 m^2/g), indicating that functionalization with 20 mL of ammonia significantly enhanced the surface development and porosity of the biochar. After adsorption, however, a substantial reduction in surface area was observed for all samples: BB decreased to 34.236 m^2/g, B20 reduced drastically to 14.899 m^2/g, and B30 declined to 18.085 m^2/g. This decline is attributed to the successful adsorption of dye molecules, which likely blocked accessible pores and

occupied available active sites, thereby reducing the overall surface area available for nitrogen adsorption during BET analysis (Mao et al., 2023).

Similarly, the total pore volume decreased for all samples after adsorption. BB decreased from 0.042 to 0.0359 cm^3/g, B20 from 0.060 to 0.0211 cm^3/g, and B30 from 0.044 to 0.0266 cm^3/g. The marked reduction in pore volume, especially in B20, supports the observation that significant pore filling occurred due to dye uptake. These reductions serve as evidence of the adsorptive interaction between the biochar surfaces and the dye molecules, confirming the materials' effectiveness as adsorbents (Goswami et al., 2022). Interestingly, an increase in the mean pore diameter was observed post-adsorption. BB increased from 3.473 to 4.199 nm, B20 from 3.298 to 5.659 nm, and B30 from 4.043 to 5.893 nm. This apparent increase in pore diameter may result from the blockage or collapse of smaller pores, leaving relatively larger pores detectable by the BET instrument. Another possibility is that some restructuring or expansion of the pore walls occurred as a result of the interaction with dye molecules during the adsorption process (Tanev & Vlaev, 1993).

Table 10: BET Surface area and pore characteristics of biochar samples after adsorption

Biochar Sample	**BET Surface Area (m^2g^{-1})**	**Total Pore Volume (cm^3g^{-1})**	**Mean Pore Diameter (nm)**
BB	34.2364	0.035940	4.1990
B20	14.8992	0.021080	5.6594
B30	18.0851	0.026646	5.8934

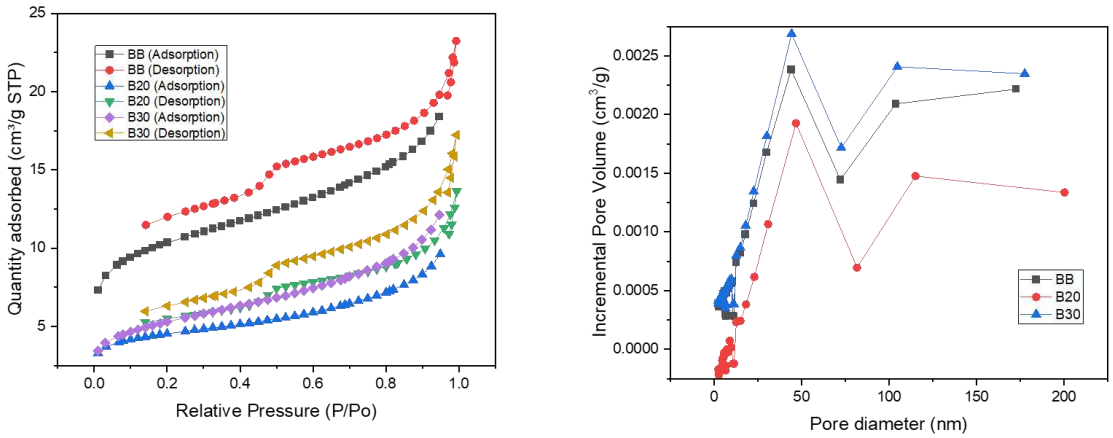


Figure 19: (a): Nitrogen adsorption-desorption isotherms of BB, B10, B20 and B30 (b): Pore size distribution of BB, B10, B20 and B30 after adsorption

5.1.6. Surface Chemical State

X-ray photoelectron spectroscopy (XPS) was employed to investigate the elemental composition and surface chemical states of the biochar before and after dye adsorption (Figure 20). Tables 11 and 12 present the XPS-derived surface elemental compositions (C1s, O1s, and N1s) and their corresponding binding energies (in eV), respectively. Before adsorption, the C1s content was relatively similar across all samples, ranging from 77.06% (BB) to 77.28% (B20) and 77.27% (B30), indicating that carbon remained the predominant surface element. Notably, N1s content was markedly increased in the ammonia-modified biochars i.e 1.90% in B20 and 2.01% in B30 compared to 0.92% in BB, confirming successful nitrogen functionalization due to ammonia treatment. The O1s content slightly decreased in the modified samples, likely due to the replacement or transformation of oxygen-containing groups during nitrogen doping (Ahmad et al., 2014; Lin et al., 2023).

After adsorption, minor but significant changes were recorded. In BB, the C1s increased marginally from 77.06% to 77.44%, while the O1s slightly decreased from 21.08% to 20.12%, suggesting surface interactions between the dye and oxygen-containing functional groups. The N1s content also reduced from 0.92% to 0.9%, implying limited nitrogen involvement in dye interaction, which aligns with BB's lower adsorption performance. For B20 and B30, the post-adsorption C1s percentages changed slightly to 74.06% and 78.09%, respectively, with O1s decreasing in B30 (to 19.07%) and increasing slightly in B20 (to 23.11%). Interestingly, the N1s content decreased from 1.90% to 1.53% in B20 and from 2.01% to 1.60% in B30, implying active participation of nitrogen-containing functional groups possibly amine or pyrrolic species in dye interaction. This supports the idea that N-functional groups introduced via ammonia treatment contributed significantly to the enhanced adsorption capacity of the modified biochars (Mahdi et al., 2019; Wu et al., 2012). The binding energy values remained relatively consistent before and after adsorption for all core levels. The C1s peaks were centered around 284.8 eV, typically associated with C–C/C=C bonds in graphitic carbon. The O1s peaks were observed around 532.4–532.6 eV, which can be attributed to oxygen in C=O, C–O, or COOH groups. These groups are known to participate in hydrogen bonding and electrostatic interactions with dye molecules, contributing to adsorption efficiency (Kambo & Dutta, 2015a) (Yin et al., 2017). The N1s peaks were located at approximately 400.0–400.2 eV, which are generally linked to pyrrolic-N, amine-N, or graphitic-N species. The slight shifts in N1s binding energy decreasing slightly post-adsorption in B20 (from 400.04 to 400.01 eV) and in B30 (from 400.09 to 399.93 eV) may suggest the formation of new surface complexes or interactions between nitrogen species and the dye's sulfonic or aromatic groups (Y. Li et al., 2014). These interactions could involve hydrogen bonding, π–π interactions, or electrostatic attractions, depending on the nature of the dye and the nitrogen configuration on the biochar surface.

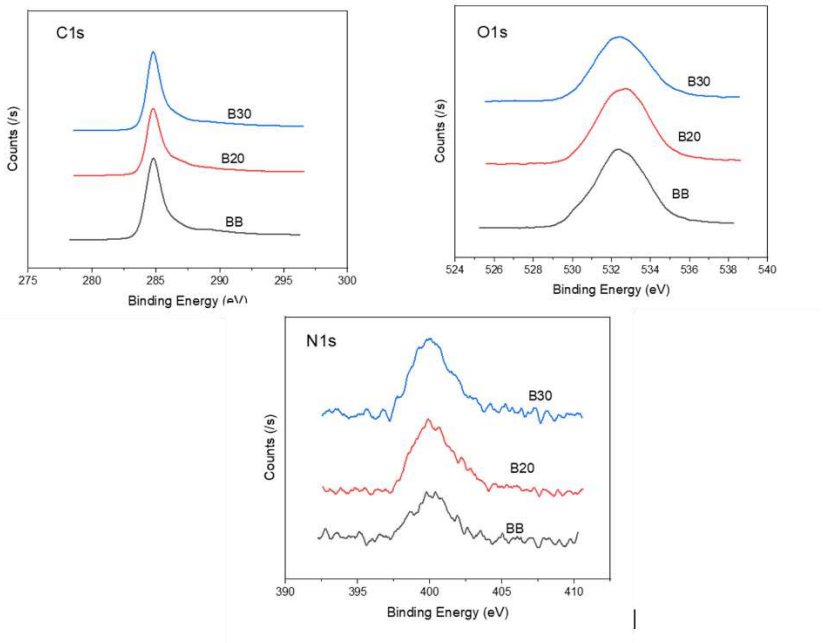


Figure 20: Binding energy analysis of C1s, O1s and N1s of BB, B10, B20 and B30 by XPS after adsorption

Table 11: XPS derived element composition (%) of the biochars after adsorption

Sample	C1s	O1s	N1s
BB	77.44	20.12	0.9
B20	74.06	23.11	1.53
B30	78.09	19.07	1.60

Table 12: XPS derived peak binding energy (eV) of the biochars after adsorption

Sample	C1s	O1s	N1s
BB	284.8	532.45	400.21
B20	284.8	532.59	400.01
B30	284.8	532.41	399.93

6. Comparative Study

The focus of this study has been to develop a high-performance adsorbent from a sustainable and low-cost feedstock. To contextualize these findings and demonstrate the practical significance of this work, the performance of the functionalized biochar was compared to that of other biochars (table 13) and that of widely used commercial adsorbents such as activated carbon (AC) and a strong-base ion-exchange resin (table 14).

Table 13: Comparison of adsorption capacity (qmax)of RB5 dye with other biochars

Biochar	Optimal Experimental Conditions	$q_{max_}$ (mg/g)	Ref.
Macadamia seed husk	pH= 3; Duration of exposure =510 min	1.21	(Felista et al., 2020)
Potato peel	pH= 3; Duration of exposure =120 min	3.61	(Samarghandy et al., 2011)
Coconut shell	pH= 2; Duration of exposure =60 min	0.82	(Tomasz Jóźwiak et al., 2018)
Pumpkin seed husk	pH= 3; Duration of exposure =60 min	1	(Kowalkowska & Jóźwiak, 2019)
Cotton fibres	pH= 3; Duration of exposure =240 min	2.74	(T Jóźwiak et al., 2020)
Wood waste	Temperature= 25^0C; Duration of exposure =90 min	35.67	(do Nascimento et al., 2021)
Eggshells	pH= 6; Duration of exposure =15 min	18.46	(Çelebi, 2019)
Fly ash	pH= 5.64; Duration of exposure =60 min	7.94	(Eren & Acar, 2006)
Banana peel	pH= 3; Duration of exposure =120 min	7.58	(Kapoor et al., 2022)
This work	pH =3; Duration of exposure = 120 min	40.91	

Table 14: Comparison of adsorption capacity (qmax)of RB5 dye with other adsorbents

Adsorbent	Q_{max} (mg/g)	Ref.
B30	40.91	This work
Activated Carbon (AC)	239.1	(Vojnović et al., 2022)
Anion Exchange Resin	1295.93	(Greluk & Hubicki, 2010)

The data clearly shows that while commercial adsorbents, such as activated carbon and ion-exchange resins, have high adsorption capacities for RB5, our functionalized biochar with a qm of 40 mg/g is highly competitive. Furthermore, the cost-effectiveness is a key advantage. The raw materials used in this study, namely bamboo waste, are significantly less expensive than the specialized, manufactured materials required for commercial activated carbon and ion-exchange resins. The superior performance of these commercial alternatives is due to their large surface area and high degree of microporosity. Activated carbon, for instance, can have a surface area of over 1000 m^2/g. Ion-exchange resins, with their specific functional groups, are engineered for high-selectivity and capacity for anionic dyes. However, the ability of our low-cost, sustainably-sourced biochar to achieve a competitive performance makes it a highly promising and economically viable alternative for industrial wastewater treatment. It offers a clear path toward a more economical and environmentally friendly solution.

7. Conclusion

This study aimed to develop efficient carbon-based adsorbent materials derived from *Bambusa vulgaris* biochar and assess their effectiveness in removing Reactive Black 5 (RB5) dye from aqueous solutions. Hydrothermal ammonia treatment successfully functionalized *Bambusa vulgaris* biochar, significantly increasing its surface nitrogen content and introducing various nitrogen-containing functional groups. This modification was crucial for enhancing the biochar's surface chemistry and improving its ability to interact with the dye. A critical assessment of these carbon-based adsorbents was presented in terms of their physicochemical properties, characterized extensively using techniques such as Scanning Electron Microscopy (SEM) for morphological analysis, Fourier Transform Infrared (FTIR) Spectroscopy for identifying surface functional groups, Thermogravimetric Analysis (TGA) for thermal stability, Elemental Analysis (CHN) for elemental composition, and X-ray Photoelectron Spectroscopy (XPS) for surface chemical states. The characterization results confirmed the successful modification of the biochar surface. SEM analysis revealed significant changes in surface morphology, including increased roughness and enhanced porosity. FTIR spectroscopy provided clear evidence of the incorporation of new functional groups, such as nitrogen-containing species (amines, amides) from ammonia, which are crucial for dye adsorption. Elemental analysis (CHN) further corroborated the successful nitrogen doping in the functionalized biochar, with variations in C, H, N, and O content reflecting the different modification strategies. TGA demonstrated that functionalization generally enhanced the thermal stability of the biochar. Finally, XPS provided detailed insights into the surface elemental composition and chemical states, confirming the specific types of nitrogen functionalities directly linking these surface properties to their potential for enhanced dye removal.

The adsorption capacity for all biochar increased with increasing initial dye concentration, driven by the higher concentration gradient. Both B20 and B30 consistently showed substantially higher adsorption capacities than BB across the tested concentration range, confirming the effectiveness of ammonia functionalization in enhancing dye uptake. B20 generally demonstrated the highest capacity, suggesting an optimal balance of functionalization and textural properties. All biochar adsorbents exhibited a rapid initial adsorption phase, followed by a slower approach to equilibrium, which was generally achieved within 120 minutes. Solution pH was identified as a critical factor, with optimal RB5 dye adsorption observed at acidic pH of 3 for all biochar. Functionalized biochar showed significantly higher adsorption capacities at acidic pH than BB, highlighting the role of introduced basic nitrogen groups. Adsorption decreased sharply at higher pH due to electrostatic repulsion. Increasing the adsorbent dose consistently led to a decrease in the adsorption capacity (qe) per unit mass for all biochar. Interestingly, BB exhibited a higher qe at lower doses compared to B20 and B30 in this specific

experiment, indicating a complex interplay between functionalization, surface properties, and the experimental conditions on the capacity per unit mass.

The adsorption of RB5 dye onto the tested biochar (BB, B20, B30) was found to be a complex process involving multiple mechanisms. These included strong electrostatic attraction, hydrogen bonding between polar groups, π-π interactions between aromatic structures of the dye and biochar, and physical pore filling within the biochar's porous network. The experimental kinetic data were best described by the Pseudo-First-Order (PFO) model, indicating that the adsorption rate is primarily controlled by the number of available active sites. The equilibrium adsorption data were best fitted by the Langmuir isotherm model, suggesting that RB5 dye adsorption predominantly occurs as a monolayer on a relatively homogeneous surface. The maximum monolayer adsorption capacity (qmax) predicted by the Langmuir model significantly increased from pristine BB to the ammonia-functionalized biochar, with B30 showing the highest predicted capacity. This confirmed that functionalization effectively enhanced the biochar's capacity for RB5 dye. The favorable Freundlich 'n' values also supported the feasibility of the adsorption process.

The ammonia-functionalized biochar (B20 and B30) demonstrated promising reusability over multiple cycles. They retained a significant portion of their initial adsorption efficiency, which is a critical factor for their practical and sustainable application in wastewater treatment. Post-adsorption characterization of the tested biochar confirmed that their fundamental structural integrity and overall morphology remained largely intact even after dye uptake. This indicates their robustness and stability during the adsorption process. Post-adsorption characterization of the functionalized biochar confirmed the successful binding of dye molecules to the biochar surface. These results suggest that functionalized Bambusa vulgaris biochar possess desirable characteristics for RB5 removal and hold potential for broader applications in water treatment and remediation processes. Further research and exploration of their performance in diverse environmental settings are warranted to fully assess their suitability and expand the range of their potential applications.

Ethical Approval

Not applicable

Funding

The authors acknowledge the supports from the National Natural Science Foundation of China (42302192).

Availability of data and materials

The data that support the findings of this study are available from the corresponding author upon reasonable request.

References

Ahmad, M., Lee, S. S., Rajapaksha, A. U., Vithanage, M., Zhang, M., Cho, J. S., Lee, S.-E., & Ok, Y. S. (2013). Trichloroethylene adsorption by pine needle biochars produced at various pyrolysis temperatures. *Bioresource Technology, 143*, 615-622.

Ahmad, M., Rajapaksha, A. U., Lim, J. E., Zhang, M., Bolan, N., Mohan, D., Vithanage, M., Lee, S. S., & Ok, Y. S. (2014). Biochar as a sorbent for contaminant management in soil and water: a review. *Chemosphere, 99*, 19-33.

Aizuddin, K., Azwa, K. N., Lai, K.-S., Baharum, N. A., Thau Lym Yong, W., Hoon, L. N., Hamid, M. Z. A., Cheng, W. H., & Abdullah, J. O. (2023). Bamboo for Biomass Energy Production. *Bioresources, 18*(1).

Al-Degs, Y. S., El-Barghouthi, M. I., El-Sheikh, A. H., & Walker, G. M. (2008). Effect of solution pH, ionic strength, and temperature on adsorption behavior of reactive dyes on activated carbon. *Dyes and pigments, 77*(1), 16-23.

Al-dhawi, B. N. S., Kutty, S. R. M., Alawag, A. M., Almahbashi, N. M. Y., Al-Towayti, F. A. H., Algamili, A., Aminu, N., Al-Mekhlafi, A.-B. A., Birniwa, A. H., & Jagaba, A. H. (2023). Optimal parameters for boron recovery in a batch adsorption study: synthesis, characterization, regeneration, kinetics, and isotherm studies. *Case Studies in Chemical and Environmental Engineering, 8*, 100508.

Alfei, S., & Pandoli, O. G. (2024). Bamboo-Based Biochar: A Still Too Little-Studied Black Gold and Its Current Applications. *Journal of Xenobiotics, 14*(1), 416-451.

Alshabanat, M., Alsenani, G., & Almufarij, R. (2013). Removal of crystal violet dye from aqueous solutions onto date palm fiber by adsorption technique. *Journal of Chemistry, 2013*(1), 210239.

Amin, M., Alazba, A., & Shafiq, M. (2019). Comparative study for adsorption of methylene blue dye on biochar derived from orange peel and banana biomass in aqueous solutions. *Environmental monitoring and assessment, 191*(12), 735.

Anil, I., Gunday, S. T., Bozkurt, A., & Alagha, O. (2020). Design of crosslinked hydrogels comprising poly (vinylphosphonic acid) and bis [2-(methacryloyloxy) ethyl] phosphate as an efficient adsorbent for wastewater dye removal. *Nanomaterials, 10*(1), 131.

Antal, M. J., & Grønli, M. (2003). The art, science, and technology of charcoal production. *Industrial & Engineering Chemistry Research, 42*(8), 1619-1640.

Arrigo, R., Hävecker, M., Wrabetz, S., Blume, R., Lerch, M., McGregor, J., Parrott, E. P., Zeitler, J. A., Gladden, L. F., & Knop-Gericke, A. (2010). Tuning the acid/base properties of nanocarbons by functionalization via amination. *Journal of the American Chemical Society, 132*(28), 9616-9630.

Arslan-Alaton, I., Koba-Ucun, O., Turkten, N., Sora, I. N., & Bekbolet, M. (2023). More about Persulfate-Assisted Ferrilanthanide-Mediated Photocatalysis of Textile Industry Dye Reactive Black 5: Surface Properties and Structural Assessment. *Water, 15*(5), 906.

Atzei, D., Fantauzzi, M., Rossi, A., Fermo, P., Piazzalunga, A., Valli, G., & Vecchi, R. (2014). Surface chemical characterization of PM10 samples by XPS. *Applied surface science, 307*, 120-128.

Çelebi, H. (2019). The applicability of evaluable wastes for the adsorption of Reactive Black 5. *International Journal of Environmental Science and Technology, 16*(1), 135-146.

Chang, M., & Shih, Y.-h. (2018). Synthesis and application of magnetic iron oxide nanoparticles on the removal of Reactive Black 5: Reaction mechanism, temperature and pH effects. *Journal of environmental management, 224*, 235-242.

Chen, B., Hui, C. W., & McKay, G. (2001). Film-pore diffusion modeling and contact time optimization for the adsorption of dyestuffs on pith. *Chemical Engineering Journal, 84*(2), 77-94.

Chen, S. (2020). Catalytic graphitization of biochar to produce graphitic carbon materials.

Chien, S., & Clayton, W. (1980). Application of Elovich equation to the kinetics of phosphate release and sorption in soils. *Soil Science Society of America Journal, 44*(2), 265-268.

Crini, G., & Badot, P.-M. (2008). Application of chitosan, a natural aminopolysaccharide, for dye removal from aqueous solutions by adsorption processes using batch studies: A review of recent literature. *Progress in Polymer Science, 33*(4), 399-447.

Damahe, D., Mayilswamy, N., & Kandasubramanian, B. (2024). Biochar/metal nanoparticles-based composites for dye remediation: a review. *Hybrid Advances, 6*, 100254.

Danya, U., Sagayaraj, C., Yaazhini, J., Ramachandran, B., Aravind, J., & Muthukumaran, P. (2024). Characterization techniques for carbon-based adsorbents and carbon composites. *Physical Sciences Reviews, 9*(11), 3387-3407.

Das, R., Ali, E., & Abd Hamid, S. B. (2014). Current applications of x-ray powder diffraction-A review. *Reviews on Advanced Materials Science, 38*(2).

Davis, T. A., Volesky, B., & Mucci, A. (2003). A review of the biochemistry of heavy metal biosorption by brown algae. *Water Research, 37*(18), 4311-4330.

de Conti, M., Dey, S., Pottker, W., & La Porta, F. (2023). An overview into advantages and applications of conventional and unconventional hydro (solvo) thermal approaches for novel advanced materials design. *Materials Today Sustainability, 23*, 100458.

do Nascimento, B. F., de Araujo, C. M. B., do Nascimento, A. C., da Costa, G. R. B., Gomes, B. F. M. L., da Silva, M. P., da Silva Santos, R. K., & da Motta Sobrinho, M. A. (2021). Adsorption of reactive black 5 and basic blue 12 using biochar from gasification residues: batch tests and fixed-bed breakthrough predictions for wastewater treatment. *Bioresource Technology Reports, 15*, 100767.

Elnour, A. Y., Alghyamah, A. A., Shaikh, H. M., Poulose, A. M., Al-Zahrani, S. M., Anis, A., & Al-Wabel, M. I. (2019). Effect of pyrolysis temperature on biochar microstructural evolution, physicochemical characteristics, and its influence on biochar/polypropylene composites. *Applied Sciences, 9*(6), 1149.

Enaime, G., Wichern, M., & Lübken, M. (2023). Contribution of biochar application to the promotion of circular economy in agriculture. *Frontiers in Agronomy, 5*, 1214012.

Eren, Z., & Acar, F. N. (2006). Adsorption of Reactive Black 5 from an aqueous solution: equilibrium and kinetic studies. *Desalination, 194*(1-3), 1-10.

Felista, M. M., Wanyonyi, W. C., & Ongera, G. (2020). Adsorption of anionic dye (Reactive Black 5) using macadamia seed husks: kinetics and equilibrium studies. *Scientific African, 7*, e00283.

Foo, K. Y., & Hameed, B. H. (2010). Insights into the modeling of adsorption isotherm systems. *Chemical Engineering Journal, 156*(1), 2-10.

Freundlich, H. (1907). Über die adsorption in lösungen. *Zeitschrift für physikalische Chemie, 57*(1), 385-470.

Gao, Y., Yang, B., & Wang, Q. (2018). *Biodegradation and decolorization of dye wastewater: a review.* Paper presented at the IOP conference series: earth and environmental science.

Ge, Q., Li, P., Liu, M., Xiao, G.-m., Xiao, Z.-q., Mao, J.-w., & Gai, X.-k. (2023). Removal of methylene blue by porous biochar obtained by KOH activation from bamboo biochar. *Bioresources and Bioprocessing, 10*(1), 51.

Goswami, L., Kushwaha, A., Kafle, S. R., & Kim, B.-S. (2022). Surface modification of biochar for dye removal from wastewater. *Catalysts, 12*(8), 817.

Greluk, M., & Hubicki, Z. (2010). Kinetics, isotherm and thermodynamic studies of Reactive Black 5 removal by acid acrylic resins. *Chemical Engineering Journal, 162*(3), 919-926.

Guo, S., Zou, Z., Chen, Y., Long, X., Liu, M., Li, X., Tan, J., & Chen, R. (2023). Synergistic effect of hydrogen bonding and π-π interaction for enhanced adsorption of rhodamine B from water using corn straw biochar. *Environmental Pollution, 320*, 121060.

Gupta, S. S., & Bhattacharyya, K. G. (2011). Kinetics of adsorption of metal ions on inorganic materials: a review. *Advances in Colloid and Interface Science, 162*(1-2), 39-58.

Gürtekin, E. (2022). Removal of Reactive Red 195 from aqueous solution using chitin. *Environmental Engineering & Management Journal (EEMJ), 21*(1).

Hadi, P., Yeung, K. Y., Barford, J., An, K. J., & McKay, G. (2015). Significance of "effective" surface area of activated carbons on elucidating the adsorption mechanism of large dye molecules. *Journal of Environmental Chemical Engineering, 3*(2), 1029-1037.

Ho, Y.-S., & Mckay, G. (1998). Kinetic models for the sorption of dye from aqueous solution by wood. *Process Safety and Environmental Protection, 76*(2), 183-191.

Ho, Y. S., Ng, J., & McKay, G. (2000). Kinetics of pollutant sorption by biosorbents. *Separation and purification methods, 29*(2), 189-232.

Hossain, N., Nizamuddin, S., Griffin, G., Selvakannan, P., Mubarak, N. M., & Mahlia, T. M. I. (2020). Synthesis and characterization of rice husk biochar via hydrothermal carbonization for wastewater treatment and biofuel production. *Scientific Reports, 10*(1), 18851.

JALALI, S. M. R., & Doroudi, Z. (2020). Removal of reactive black 5 from waste waters by adsorption: a comprehensive review.

Jones, E. R., Van Vliet, M. T., Qadir, M., & Bierkens, M. F. (2021). Country-level and gridded estimates of wastewater production, collection, treatment and reuse. *Earth System Science Data, 13*(2), 237-254.

Jóźwiak, T., Filipkowska, U., Brym, S., & Kopeć, L. (2020). Use of aminated hulls of sunflower seeds for the removal of anionic dyes from aqueous solutions. *International Journal of Environmental Science and Technology, 17*(3), 1211-1224.

Jóźwiak, T., Filipkowska, U., Bugajska, P., & Kalkowski, T. (2018). The use of coconut shells for the removal of dyes from aqueous solutions. *Journal of Ecological Engineering, 19*(4), 129-135.

Jóźwiak, T., Filipkowska, U., & Walczak, P. (2022). The Use of Aminated Wheat Straw for Reactive Black 5 Dye Removal from Aqueous Solutions as a Potential Method of Biomass Valorization. *Energies, 15*(17), 6257.

Kambo, H. S., & Dutta, A. (2015a). Comparative evaluation of torrefaction and hydrothermal carbonization of lignocellulosic biomass for the production of solid biofuel. *Energy conversion and Management, 105*, 746-755.

Kambo, H. S., & Dutta, A. (2015b). A comparative review of biochar and hydrochar in terms of production, physico-chemical properties and applications. *Renewable and Sustainable Energy Reviews, 45*, 359-378.

Kapoor, R. T., Rafatullah, M., Siddiqui, M. R., Khan, M. A., & Sillanpää, M. (2022). Removal of reactive black 5 dye by banana peel biochar and evaluation of its phytotoxicity on tomato. *Sustainability, 14*(7), 4176.

Karadag, D., Turan, M., Akgul, E., Tok, S., & Faki, A. (2007). Adsorption equilibrium and kinetics of reactive black 5 and reactive red 239 in aqueous solution onto surfactant-modified zeolite. *Journal of Chemical & Engineering Data, 52*(5), 1615-1620.

Kowalkowska, A., & Jóźwiak, T. (2019). Utilization of pumpkin (Cucurbita pepo) seed husks as a low-cost sorbent for removing anionic and cationic dyes from aqueous solutions. *Desalination and Water Treatment, 171*, 397-407.

Kumari, H., Sonia, Suman, Ranga, R., Chahal, S., Devi, S., Sharma, S., Kumar, S., Kumar, P., & Kumar, S. (2023). A review on photocatalysis used for wastewater treatment: dye degradation. *Water, Air, & Soil Pollution, 234*(6), 349.

Kurniawan, A., Ismadji, S., & Zhou, C. H. (2024). Structural and Functional Modifications of Biochar for Removal of Chemical Pollutants in Wastewater Treatment *Catalytic Applications of Biochar for Environmental Remediation: A Green Approach Towards Environment Restoration (Vol 1)* (pp. 71-107): ACS Publications.

Langmuir, I. (1918). The adsorption of gases on plane surfaces of glass, mica and platinum. *Journal of the American Chemical Society, 40*(9), 1361-1403.

Ledakowicz, S., & Paździor, K. (2021). Recent achievements in dyes removal focused on advanced oxidation processes integrated with biological methods. *Molecules, 26*(4), 870.

Lehmann, J., & Joseph, S. (2015). Biochar for environmental management: an introduction *Biochar for environmental management* (pp. 1-13): Routledge.

Li, B., Wang, Q., Guo, J.-Z., Huan, W.-W., & Liu, L. (2018). Sorption of methyl orange from aqueous solution by protonated amine modified hydrochar. *Bioresource Technology, 268*, 454-459.

Li, X., Huang, Y., Liang, X., Huang, L., Wei, L., Zheng, X., Albert, H. A., Huang, Q., Liu, Z., & Li, Z. (2022). Characterization of biochars from woody agricultural wastes and sorption behavior comparison of cadmium and atrazine. *Biochar, 4*(1), 27.

Li, Y., Shao, J., Wang, X., Deng, Y., Yang, H., & Chen, H. (2014). Characterization of modified biochars derived from bamboo pyrolysis and their utilization for target component (furfural) adsorption. *Energy & Fuels, 28*(8), 5119-5127.

Li, Z., Sellaoui, L., Franco, D., Netto, M. S., Georgin, J., Dotto, G. L., Bajahzar, A., Belmabrouk, H., Bonilla-Petriciolet, A., & Li, Q. (2020). Adsorption of hazardous dyes on functionalized multiwalled carbon nanotubes in single and binary systems: Experimental study and physicochemical interpretation of the adsorption mechanism. *Chemical Engineering Journal, 389*, 124467.

Lin, Z., Wang, R., Tan, S., Zhang, K., Yin, Q., Zhao, Z., & Gao, P. (2023). Nitrogen-doped hydrochar prepared by biomass and nitrogen-containing wastewater for dye adsorption: effect of nitrogen source in wastewater on the adsorption performance of hydrochar. *Journal of environmental management, 334*, 117503.

Liu, Q., Zang, G.-L., & Zhao, Q. (2021). Removal of copper ions by functionalized biochar based on a multicomponent Ugi reaction. *RSC advances, 11*(42), 25880-25891.

Liu, Z., & Zhang, F.-S. (2011). Removal of copper (II) and phenol from aqueous solution using porous carbons derived from hydrothermal chars. *Desalination, 267*(1), 101-106.

Luo, M., Jiang, X., Liu, Y., Liu, Y., Yu, H., Niu, Y., Meng, X., Wang, L., & Niu, Y. (2023). Enhanced adsorption complexation of biochar by nitrogen-containing functional groups. *Journal of Environmental Chemical Engineering, 11*(6), 111194.

Mahbub, S., Shahriar, I., Iqfath, M., Hoque, M. A., Halim, M. A., Khan, M. A., Rub, M. A., & Asiri, A. M. (2019). Influence of alcohols/electrolytes on the interaction of reactive red dye with surfactant and removal of dye from solutions. *Journal of Environmental Chemical Engineering, 7*(5), 103364.

Mahdi, Z., El Hanandeh, A., & Yu, Q. J. (2019). Preparation, characterization and application of surface modified biochar from date seed for improved lead, copper, and nickel removal from aqueous solutions. *Journal of Environmental Chemical Engineering, 7*(5), 103379.

Mao, Y., Cai, B., Huang, M., Liu, X., Zhang, W., & Ma, Z. (2023). A sustainable preparation strategy for the nitrogen-doped hierarchical biochar with high surface area for the enhanced removal of organic dye. *Biochar, 5*(1), 70.

Mehra, S., Singh, M., & Chadha, P. (2021). Adverse impact of textile dyes on the aquatic environment as well as on human beings. *Toxicol. Int, 28*(2), 165.

Mohan, D., Pittman Jr, C. U., & Steele, P. H. (2006). Pyrolysis of wood/biomass for bio-oil: a critical review. *Energy & Fuels, 20*(3), 848-889.

Moradihamedani, P. (2022). Recent advances in dye removal from wastewater by membrane technology: a review. *Polymer Bulletin, 79*(4), 2603-2631.

Murphy, O. P., Vashishtha, M., Palanisamy, P., & Kumar, K. V. (2023). A review on the adsorption isotherms and design calculations for the optimization of adsorbent mass and contact time. *ACS omega, 8*(20), 17407-17430.

Ndoun, M. C., Knopf, A., Preisendanz, H. E., Vozenilek, N., Elliott, H. A., Mashtare, M. L., Velegol, S., Veith, T. L., & Williams, C. F. (2023). Physicochemical characterization of biochar derived from the pyrolysis of cotton gin waste and walnut shells. *Journal of the ASABE*, 0.

Nematollahzadeh, A., Shojaei, A., & Karimi, M. (2015). Chemically modified organic/inorganic nanoporous composite particles for the adsorption of reactive black 5 from aqueous solution. *Reactive and Functional Polymers, 86*, 7-15.

Niazi, N. K., Murtaza, B., Bibi, I., Shahid, M., White, J., Nawaz, M., Bashir, S., Shakoor, M., Choppala, G., & Murtaza, G. (2016). Removal and recovery of metals by biosorbents and biochars derived from biowastes *Environmental materials and waste* (pp. 149-177): Elsevier.

Obodo, K., & Aigbe, U. O. (2023). The types, characteristics, and management options (reusability/recyclability/final disposal) of commonly used adsorbents in environmental sustainability *Adsorption Applications for Environmental Sustainability* (pp. 2-1-2-25): IOP Publishing Bristol, UK.

Oswald, S. (2006). X-ray photoelectron spectroscopy in analysis of surfaces. *Encyclopedia of Analytical Chemistry: Applications, Theory and Instrumentation*.

Ovchinnikov, O. V., Evtukhova, A. V., Kondratenko, T. S., Smirnov, M. S., Khokhlov, V. Y., & Erina, O. V. (2016). Manifestation of intermolecular interactions in FTIR spectra of methylene blue molecules. *Vibrational Spectroscopy, 86*, 181-189.

Park, J.-H., Wang, J. J., Meng, Y., Wei, Z., DeLaune, R. D., & Seo, D.-C. (2019). Adsorption/desorption behavior of cationic and anionic dyes by biochars prepared at normal and high pyrolysis temperatures. *Colloids and Surfaces A: Physicochemical and Engineering Aspects, 572*, 274-282.

Peng, Y., He, S., & Wu, F. (2021). Biochemical processes mediated by iron-based materials in water treatement: enhancing nitrogen and phosphorus removal in low C/N ratio wastewater. *Science of the total environment, 775*, 145137.

Qin, L., Feng, L., Li, C., Fan, Z., Zhang, G., Shen, C., & Meng, Q. (2019). Amination/oxidization dual-modification of waste ginkgo shells as bio-adsorbents for copper ion removal. *Journal of cleaner production, 228*, 112-123.

Ranjan, R., Thust, S., Gounaris, C. E., Woo, M., Floudas, C. A., von Keitz, M., Valentas, K. J., Wei, J., & Tsapatsis, M. (2009). Adsorption of fermentation inhibitors from lignocellulosic biomass hydrolyzates for improved ethanol yield and value-added product recovery. *Microporous and Mesoporous Materials, 122*(1-3), 143-148.

Rashid, R., Shafiq, I., Akhter, P., Iqbal, M. J., & Hussain, M. (2021). A state-of-the-art review on wastewater treatment techniques: the effectiveness of adsorption method. *Environmental Science and Pollution Research, 28*, 9050-9066.

Saad, I., Ralha, N., Abukhadra, M. R., Al Zoubi, W., & Ko, Y. G. (2023). Recent advances in photocatalytic oxidation techniques for decontamination of water. *Journal of Water Process Engineering, 52*, 103572.

Sajjadi, B., Zubatiuk, T., Leszczynska, D., Leszczynski, J., & Chen, W. Y. (2019). Chemical activation of biochar for energy and environmental applications: a comprehensive review. *Reviews in Chemical Engineering, 35*(7), 777-815.

Samarghandy, M. R., Hoseinzadeh, E., Taghavi, M., & Rahmani, A. (2011). Biosorption of reactive black 5 from aqueous solution using acid-treated biomass of potato peel waste. *Bioresources, 6*(4), 4840-4855.

Sekhon, S. S., & Park, J.-S. (2021). Biomass-derived N-doped porous carbon nanosheets for energy technologies. *Chemical Engineering Journal, 425*, 129017.

Shokohi, R., Samarghandi, M., Pourfarzi, F., Siboni, M. S., & Vahedi, H. (2011). Removal of reactive black 5 (RB5) dye from aquatic solution by using of adsorption onto synthesized sodiumalginate magnetic beads.

Sing, K. (2001). The use of nitrogen adsorption for the characterisation of porous materials. *Colloids and Surfaces A: Physicochemical and Engineering Aspects, 187*, 3-9.

Singh, A., Sharma, R., Pant, D., & Malaviya, P. (2021). Engineered algal biochar for contaminant remediation and electrochemical applications. *Science of the total environment, 774*, 145676.

Sutradhar, S., Mondal, A., Kuehne, F., Krueger, O., Rakshit, S. K., & Kang, K. (2024). Comparison of oil-seed shell biomass-based biochar for the removal of anionic dyes—characterization and adsorption efficiency studies. *Plants, 13*(6), 820.

Tan, X.-F., Zhu, S.-S., Wang, R.-P., Chen, Y.-D., Show, P.-L., Zhang, F.-F., & Ho, S.-H. (2021). Role of biochar surface characteristics in the adsorption of aromatic compounds: Pore structure and functional groups. *Chinese Chemical Letters, 32*(10), 2939-2946.

Tan, Z., Yuan, S., Hong, M., Zhang, L., & Huang, Q. (2020). Mechanism of negative surface charge formation on biochar and its effect on the fixation of soil Cd. *Journal of hazardous materials, 384*, 121370.

Tanev, P. T., & Vlaev, L. T. (1993). An attempt at a more precise evaluation of the approach to mesopore size distribution calculations depending on the degree of pore blocking. *Journal of colloid and interface science, 160*(1), 110-116.

Tang, L., Chen, S., Wang, N., & Jiang, X. (2025). Comparative study of adsorption and slow-release performance and mechanism of phosphoric acid and ammonia-modified biochars on 2, 4-dichlorophenoxyacetic acid. *Separation and Purification Technology, 358*, 130470.

Uddin, M. J., Ampiaw, R. E., & Lee, W. (2021). Adsorptive removal of dyes from wastewater using a metal-organic framework: A review. *Chemosphere, 284*, 131314.

Verma, A. K., Dash, R. R., & Bhunia, P. (2012). A review on chemical coagulation/flocculation technologies for removal of colour from textile wastewaters. *Journal of environmental management, 93*(1), 154-168.

Vojnović, B., Cetina, M., Franjković, P., & Sutlović, A. (2022). Influence of initial pH value on the adsorption of reactive black 5 dye on powdered activated carbon: kinetics, mechanisms, and thermodynamics. *Molecules, 27*(4), 1349.

Wang, J., & Guo, X. (2020). Adsorption isotherm models: Classification, physical meaning, application and solving method. *Chemosphere, 258*, 127279.

Wang, L., Yang, H., Dong, Y., Chen, E., & Tang, S. (2018). Environmental evaluation, hydration, pore structure, volume deformation and abrasion resistance of low heat Portland (LHP) cement-based materials. *Journal of cleaner production, 203*, 540-558.

Wang, S., Li, X., Liu, Y., Zhang, C., Tan, X., Zeng, G., Song, B., & Jiang, L. (2018). Nitrogen-containing amino compounds functionalized graphene oxide: synthesis, characterization and application for the removal of pollutants from wastewater: a review. *Journal of hazardous materials, 342*, 177-191.

Wekoye, J. N., Wanyonyi, W. C., Wangila, P. T., & Tonui, M. K. (2020). Kinetic and equilibrium studies of Congo red dye adsorption on cabbage waste powder. *Environmental chemistry and ecotoxicology, 2*, 24-31.

Wong, S., Ghafar, N. A., Ngadi, N., Razmi, F. A., Inuwa, I. M., Mat, R., & Amin, N. A. S. (2020). Effective removal of anionic textile dyes using adsorbent synthesized from coffee waste. *Scientific Reports, 10*(1), 2928.

Wu, W., Yang, M., Feng, Q., McGrouther, K., Wang, H., Lu, H., & Chen, Y. (2012). Chemical characterization of rice straw-derived biochar for soil amendment. *Biomass and bioenergy, 47*, 268-276.

Xie, J., Lin, R., Liang, Z., Zhao, Z., Yang, C., & Cui, F. (2021). Effect of cations on the enhanced adsorption of cationic dye in Fe3O4-loaded biochar and mechanism. *Journal of Environmental Chemical Engineering, 9*(4), 105744.

Xue, Y., Hou, H., & Zhu, S. (2009). Adsorption removal of reactive dyes from aqueous solution by modified basic oxygen furnace slag: isotherm and kinetic study. *Chemical Engineering Journal, 147*(2-3), 272-279.

Yagub, M. T., Sen, T. K., Afroze, S., & Ang, H. M. (2014). Dye and its removal from aqueous solution by adsorption: a review. *Advances in Colloid and Interface Science, 209*, 172-184.

Yakout, S. M. (2017). Physicochemical characteristics of biochar produced from rice straw at different pyrolysis temperature for soil amendment and removal of organics. *Proceedings of the National Academy of Sciences, India Section A: Physical Sciences, 87*, 207-214.

Yang, J., Pignatello, J. J., Yang, K., Wu, W., Lu, G., Zhang, L., Yang, C., & Dang, Z. (2021). Adsorption of organic compounds by biomass chars: direct role of aromatic condensation (ring cluster size) revealed by experimental and theoretical studies. *Environmental science & technology, 55*(3), 1594-1603.

Yang, X.-Y., & Al-Duri, B. (2001). Application of branched pore diffusion model in the adsorption of reactive dyes on activated carbon. *Chemical Engineering Journal, 83*(1), 15-23.

Yin, Q., Zhang, B., Wang, R., & Zhao, Z. (2017). Biochar as an adsorbent for inorganic nitrogen and phosphorus removal from water: a review. *Environmental Science and Pollution Research, 24*, 26297-26309.

Yuan, X., Cao, Y., Li, J., Patel, A. K., Dong, C.-D., Jin, X., Gu, C., Yip, A. C., Tsang, D. C., & Ok, Y. S. (2023). Recent advancements and challenges in emerging applications of biochar-based catalysts. *Biotechnology advances, 67*, 108181.

Zaheer, Z., Aisha, A.-A., & Aazam, E. S. (2019). Adsorption of methyl red on biogenic Ag@ Fe nanocomposite adsorbent: Isotherms, kinetics and mechanisms. *Journal of Molecular Liquids, 283*, 287-298.

Zaman, S., Sen, S., Fatema, M. K., Haque, S., Asif, S. M. H., Abu Rayhan, M., Biswas, A., Sarker, S., Hasan, M. J., & Ahmmed, M. (2025). Adsorption of Reactive Red 120 dye from simulated wastewater using rice straw charcoal: isotherm and kinetic studies. *H2Open Journal, 8*(3), 89-99.

Zhang, C., Liu, L., Zhao, M., Rong, H., & Xu, Y. (2018). The environmental characteristics and applications of biochar. *Environmental Science and Pollution Research, 25*, 21525-21534.

Zhang, X., Zhang, S., Yang, H., Feng, Y., Chen, Y., Wang, X., & Chen, H. (2014). Nitrogen enriched biochar modified by high temperature CO2–ammonia treatment: characterization and adsorption of CO2. *Chemical Engineering Journal, 257*, 20-27.

Zhang, Z., Cao, B., Chen, Z., & Xu, K. (2022). Grafting enhances the photosynthesis and nitrogen absorption of tomato plants under low-nitrogen stress. *Journal of Plant Growth Regulation, 41*(4), 1714-1725.

Zhao, C., Zhang, W., Zhang, Y., Yang, Y., Guo, D., Liu, W., & Liu, L. (2024). Influence of multivalent background ions competition adsorption on the adsorption behavior of azo dye molecules and removal mechanism: Based on machine learning, DFT and experiments. *Separation and Purification Technology, 341*, 126810.

Zheng, Q., Dai, Y., & Han, X. (2016). Decolorization of azo dye CI Reactive Black 5 by ozonation in aqueous solution: influencing factors, degradation products, reaction pathway and toxicity assessment. *Water Science and Technology, 73*(7), 1500-1510.

Zhou, X., Zhou, J., Liu, Y., Guo, J., Ren, J., & Zhou, F. (2018). Preparation of iminodiacetic acid-modified magnetic biochar by carbonization, magnetization and functional modification for Cd (II) removal in water. *Fuel, 233*, 469-479.

Zhu, Y., Liang, H., Yu, R., Hu, G., & Chen, F. (2020). Removal of aquatic cadmium ions using thiourea modified poplar biochar. *Water, 12*(4), 1117.